

# Disentangling the high- and low-cutoff scales via the trilinear Higgs couplings in the type I two-Higgs-doublet model

Sin Kyu Kang,<sup>1,\*</sup> Jinheung Kim,<sup>2,†</sup> Soojin Lee,<sup>2,‡</sup> and Jeonghyeon Song<sup>2,§</sup>

<sup>1</sup>*School of Natural Science, Seoul National University  
of Science and Technology, Seoul 139-743, Korea*

<sup>2</sup>*Department of Physics, Konkuk University, Seoul 05029, Republic of Korea*

## Abstract

The type I two-Higgs-doublet model in the inverted Higgs scenario can retain the theoretical stability all the way up to the Planck scale. The Planck-scale cutoff,  $\Lambda_{\text{cut}}^{\text{Planck}}$ , directly impacts the mass spectra such that all the extra Higgs boson masses should be light below about 160 GeV. However, the observation of the light masses of new Higgs bosons does not indicate the high-cutoff scale because a low-cutoff scale can also accommodate the light masses. Over the viable parameter points that satisfy the theoretical requirements and the experimental constraints, we show that the trilinear Higgs couplings for low  $\Lambda_{\text{cut}}$  are entirely different from those for the Planck-scale cutoff. The most sensitive coupling to the cutoff scale is from the  $h$ - $h$ - $h$  vertex, where  $h$  is the lighter  $CP$ -even Higgs boson at a mass below 125 GeV. The gluon fusion processes of  $gg \rightarrow hh$  and  $gg \rightarrow AA$  are insensitive to the cutoff scale, yielding a small variation of the production cross sections,  $\mathcal{O}(1)$  fb, according to  $\Lambda_{\text{cut}}$ . The smoking-gun signature is from the triple Higgs production of  $q\bar{q}' \rightarrow W^* \rightarrow H^\pm hh$ , which solely depends on the  $h$ - $h$ - $h$  vertex. The cross section for  $\Lambda_{\text{cut}} = 1$  TeV is about  $10^3$  times larger than that for the Planck-scale cutoff. Since the decay modes of  $H^\pm \rightarrow W^*h/W^*A$  and  $h/A \rightarrow bb$  are dominant, the process yields the  $6b + \ell\nu$  final state, which enjoys an almost background-free environment. Consequently, the precision measurement of  $pp \rightarrow H^\pm hh$  can probe the cutoff scale of the model.

arXiv:2210.00020v3 [hep-ph] 19 Jan 2023

---

\*Electronic address: [skkang@snut.ac.kr](mailto:skkang@snut.ac.kr)

†Electronic address: [jinheung.kim1216@gmail.com](mailto:jinheung.kim1216@gmail.com)

‡Electronic address: [soojinlee957@gmail.com](mailto:soojinlee957@gmail.com)

§Electronic address: [jhsong@konkuk.ac.kr](mailto:jhsong@konkuk.ac.kr)

## Contents

I. Introduction	2
II. Review of type I of 2HDM in the inverted scenario	4
III. Scanning and RGE analysis	6
IV. Trilinear Higgs couplings	10
V. LHC phenomenology	13
VI. Conclusion	18
Acknowledgments	19
A. RGEs in the type I	19
References	21

## I. INTRODUCTION

Up to today, all of the measurements of the production cross sections of the standard model (SM) particles at high-energy colliders are in good agreement with the SM predictions [1], including the observed Higgs boson with a mass of 125 GeV [2–16]. Nevertheless, our minds are rarely in satisfaction with the SM, because of the unsolved questions such as the naturalness problem, baryogenesis, non-zero neutrino masses, fermion mass hierarchy, the origin of  $CP$  violation in the quark sector, and the identity of dark matter. We continue our journey in the quest for the ultimate theory.

A crucial question is whether the ultimate theory shall reveal its whole structure at one energy scale. The answer is much more likely to be *no* when looking back on the SM, the only reliable guideline at this moment. We witnessed the emergence of SM particles in stages. The same phenomena could happen in the ultimate theory. In other words, the final theory may consist of multilevel sub-models. The first-stage NP model<sup>1</sup> describes our universe up to a particular energy scale  $\Lambda_{\text{cut}}$  and then hands over its role to the second-stage NP model.  $\Lambda_{\text{cut}}$  could be as high as the Planck scale or as low as 10 TeV. Then can an observable distinguish the high and low  $\Lambda_{\text{cut}}$ ? This is the driving question in our paper.

For the first-stage NP model, we consider the two-Higgs-doublet model (2HDM) since many fundamental questions are closely related to the Higgs sector. The 2HDM provides the answers

---

<sup>1</sup> Two different structures exist for the first-stage NP model. It can take over the SM from a high-energy scale, accommodating new heavy particles with the multi-TeV masses. Or it coexists with the SM at the electroweak scale so that the new particles have the intermediate masses.

to some questions. For example, the first-order electroweak phase transition in the 2HDM can explain the baryogenesis [17–21]. However, the model cannot address all the fundamental questions, which makes it a suitable candidate for the first-stage NP model.

Then the next question is how to calculate the energy scale at which the second-stage NP model appears. A good way is to calculate the cutoff scale of the 2HDM. Even though the theoretical requirements (unitarity, perturbativity, and vacuum stability) are satisfied at the electroweak scale, they can be broken at a higher energy scale  $\Lambda_{\text{cut}}$  because the parameters evolve under renormalization group equations (RGE) [22–28]. Since it implies the advent of the second-stage NP model, we call  $\Lambda_{\text{cut}}$  the cutoff scale of the model.

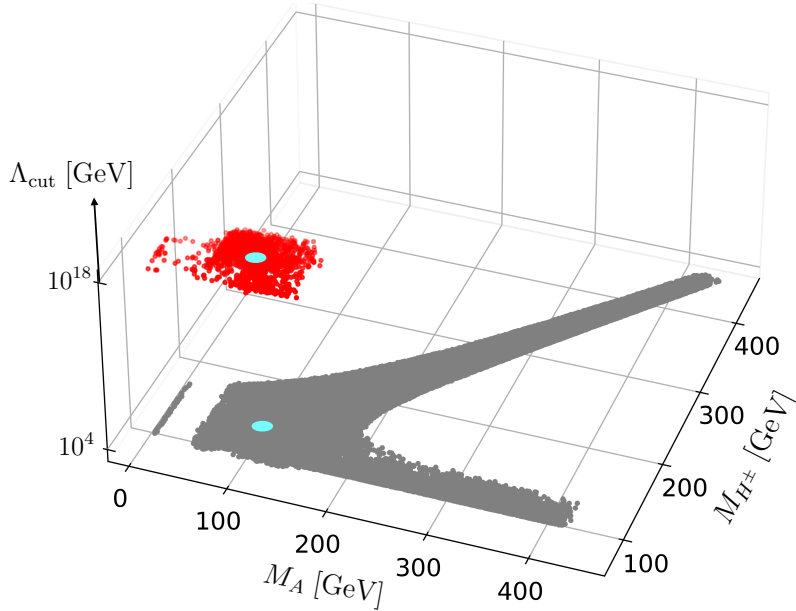


FIG. 1: Allowed  $(M_A, M_{H^\pm})$  with the cutoff scales of  $\Lambda_{\text{cut}} = 10 \text{ TeV}$  (gray points) and  $\Lambda_{\text{cut}} = 10^{18} \text{ GeV}$  (red points) in the inverted type I, over the viable parameter points that satisfy the theoretical requirements and the experimental constraints. Two points in cyan yield the same  $M_A$  and  $M_{H^\pm}$ .

In the literature, the high-energy scale behavior of the 2HDM has been extensively studied. Most studies are focused on the impact of high  $\Lambda_{\text{cut}}$  on the extra Higgs boson masses [26, 29–37]. However, observing the scalar mass spectrum that high  $\Lambda_{\text{cut}}$  predicts does not guarantee that  $\Lambda_{\text{cut}}$  is high. In this paper, we focus on the type I of the 2HDM in the inverted Higgs scenario where the heavier  $CP$ -even scalar  $H$  is the observed Higgs boson [38–40]. The model can accommodate the cutoff scale all the way up to the Planck scale [35]. As illustrated in Fig. 1, the allowed points of  $(M_A, M_{H^\pm})$  for  $\Lambda_{\text{cut}} = 10^{18} \text{ GeV}$  (red points) are overlapped with those for  $\Lambda_{\text{cut}} = 10 \text{ TeV}$  (gray points). Two points in cyan, one for  $\Lambda_{\text{cut}} = 10 \text{ TeV}$  and the other for  $\Lambda_{\text{cut}} = 10^{18} \text{ GeV}$ , have the same  $M_A$  and  $M_{H^\pm}$ . We need an alternative observable to disentangle the high- and low-cutoff scales. The measurement of  $\tan \beta$ , the ratio of two vacuum expectation values of two Higgs doublet fields, is tricky in type I when  $\tan \beta$  is large. In type

I, all the Yukawa couplings of the BSM Higgs bosons are inversely proportional to  $\tan\beta$  in the Higgs alignment limit. So, the main production channels of  $gg \rightarrow A/h$  and  $t \rightarrow H^\pm b$  are suppressed by large  $\tan\beta$ . In addition, the branching ratios of all the fermionic decay modes are insensitive to  $\tan\beta$  in type I. We need alternative observables to probe the cutoff scale.

We will show that the trilinear Higgs couplings can play the role. In particular, the value of the  $h$ - $h$ - $h$  vertex,  $\lambda_{hhh}$ , is highly sensitive to the cutoff scale. To probe the trilinear Higgs couplings at the LHC, we will study the di-Higgs processes of  $gg \rightarrow hh$  and  $gg \rightarrow AA$ , and the tri-Higgs processes of  $pp \rightarrow H^\pm hh$ . The gluon fusion production of  $gg \rightarrow h/H \rightarrow hh/AA$  is to be shown insensitive to  $\Lambda_{\text{cut}}$  because of the destructive interference between the  $h$  and  $H$  contributions. We will show that the tri-Higgs process  $pp \rightarrow H^\pm hh$  is the best to measure the cutoff scale because the signal rate is solely dependent on  $\lambda_{hhh}$ , yielding  $\sigma_{\Lambda_{\text{cut}}=1 \text{ TeV}}/\sigma_{\Lambda_{\text{cut}}=10^{18} \text{ GeV}} \sim 10^3$ . Considering the dominant decays modes of  $H^\pm$  and  $h$ , we will suggest for the first time the  $6b + \ell\nu$  final state as an efficient discriminator between the high- and low-cutoff scales. These are our new contributions.

The paper is organized in the following way. In Sec. II, we briefly review the type I in the inverted scenario. Section III describes the methods of the parameter scanning and the calculation of  $\Lambda_{\text{cut}}$ . The characteristics of the viable parameter points with high  $\Lambda_{\text{cut}}$  are also presented. In Sec. IV, we calculate the correlation between the trilinear Higgs couplings and the cutoff scale. Section V deals with the LHC phenomenology. Based on the study of the branching ratios of the extra Higgs bosons, we will suggest efficient observables to distinguish the high- and low-cutoff scales. Finally we conclude in Sec. VI.

## II. REVIEW OF TYPE I OF 2HDM IN THE INVERTED SCENARIO

The 2HDM introduces two  $SU(2)_L$  complex scalar doublet fields with hypercharge  $Y = 1$ ,  $\Phi_1$  and  $\Phi_2$  [41]:

$$\Phi_i = \begin{pmatrix} w_i^+ \\ \frac{v_i + \rho_i + i\eta_i}{\sqrt{2}} \end{pmatrix}, \quad (i = 1, 2) \quad (1)$$

where  $v_1$  and  $v_2$  are the nonzero vacuum expectation values of  $\Phi_1$  and  $\Phi_2$ , respectively. The ratio of  $v_2/v_1$  defines the mixing angle  $\beta$  via  $\tan\beta = v_2/v_1$ . For notational simplicity, we use  $s_x = \sin x$ ,  $c_x = \cos x$ , and  $t_x = \tan x$  in what follows. The combination of  $v_1$  and  $v_2$ ,  $v = \sqrt{v_1^2 + v_2^2} = 246 \text{ GeV}$ , spontaneously breaks the electroweak symmetry. To prevent flavor-changing neutral currents at tree level, we impose a discrete  $Z_2$  symmetry under which  $\Phi_1 \rightarrow \Phi_1$  and  $\Phi_2 \rightarrow -\Phi_2$  [42, 43]. We allow softly broken  $Z_2$  symmetry since it does not affect the RGE of the dimensionless quartic couplings [44]: the hard  $Z_2$  breaking in the Yukawa sector causes too fast growth of the scalar quartic couplings in the RG running [32].

For simplicity, we employ a  $CP$ -conserving scalar potential that softly breaks the  $Z_2$  sym-

metry, which is given by

$$\begin{aligned}
V_{\Phi} = & m_{11}^2 \Phi_1^\dagger \Phi_1 + m_{22}^2 \Phi_2^\dagger \Phi_2 - m_{12}^2 (\Phi_1^\dagger \Phi_2 + \text{H.c.}) \\
& + \frac{1}{2} \lambda_1 (\Phi_1^\dagger \Phi_1)^2 + \frac{1}{2} \lambda_2 (\Phi_2^\dagger \Phi_2)^2 + \lambda_3 (\Phi_1^\dagger \Phi_1) (\Phi_2^\dagger \Phi_2) + \lambda_4 (\Phi_1^\dagger \Phi_2) (\Phi_2^\dagger \Phi_1) \\
& + \frac{1}{2} \lambda_5 \left[ (\Phi_1^\dagger \Phi_2)^2 + \text{H.c.} \right],
\end{aligned} \tag{2}$$

where the  $m_{12}^2$  term softly breaks the  $Z_2$  symmetry. The scalar potential  $V_{\Phi}$  yields five physical Higgs bosons, the lighter  $CP$ -even scalar  $h$ , the heavier  $CP$ -even scalar  $H$ , the  $CP$ -odd pseudoscalar  $A$ , and a pair of charged Higgs bosons  $H^{\pm}$ . Relations of mass eigenstates with weak eigenstates in terms of two mixing angles of  $\alpha$  and  $\beta$  are referred to Ref. [45]. The SM Higgs boson is a linear combination of  $h$  and  $H$ , given by

$$h_{\text{SM}} = s_{\beta-\alpha} h + c_{\beta-\alpha} H. \tag{3}$$

The observed Higgs boson at a mass of 125 GeV at the LHC [2–16] has so far agreed with the predictions for the SM Higgs boson. The SM-like Higgs boson strongly motivates the Higgs alignment limit in the 2HDM. Two scenarios exist for the limit, the normal scenario where  $h_{\text{SM}} = h$  (i.e.,  $s_{\beta-\alpha} = 1$ ) and the inverted scenario where  $h_{\text{SM}} = H$  (i.e.,  $c_{\beta-\alpha} = 1$ ). In this paper, we concentrate on the inverted scenario in the Higgs alignment limit:

$$M_H = 125 \text{ GeV}, \quad c_{\beta-\alpha} = 1. \tag{4}$$

Then we have the following five parameters:

$$\{m_h, \quad M_A, \quad M_{H^{\pm}}, \quad t_{\beta}, \quad m_{12}^2\}, \tag{5}$$

which define one parameter point. Then, the quartic coupling constants in  $V_{\Phi}$  are written as [46]

$$\begin{aligned}
\lambda_1 &= \frac{1}{v^2} [m_{125}^2 + t_{\beta}^2 (m_h^2 - M^2)], \\
\lambda_2 &= \frac{1}{v^2} \left[ m_{125}^2 + \frac{1}{t_{\beta}^2} (m_h^2 - M^2) \right], \\
\lambda_3 &= \frac{1}{v^2} [m_{125}^2 - m_h^2 - M^2 + 2M_{H^{\pm}}^2], \\
\lambda_4 &= \frac{1}{v^2} [M^2 + M_A^2 - 2M_{H^{\pm}}^2], \\
\lambda_5 &= \frac{1}{v^2} [M^2 - M_A^2],
\end{aligned} \tag{6}$$

where  $m_{125} = 125 \text{ GeV}$  and  $M^2 = m_{12}^2 / (s_{\beta} c_{\beta})$ .

The Yukawa couplings to the SM fermions are parametrized as

$$\begin{aligned}
\mathcal{L}^{\text{Yuk}} = & - \sum_f \left( \frac{m_f}{v} \xi_f^h \bar{f} f h + \frac{m_f}{v} \kappa_f^H \bar{f} f H - i \frac{m_f}{v} \xi_f^A \bar{f} \gamma_5 f A \right) \\
& - \left\{ \frac{\sqrt{2}}{v} \bar{t} (m_t \xi_t^A P_- + m_b \xi_b^A P_+) b H^+ + \frac{\sqrt{2} m_{\tau}}{v} \xi_{\tau}^A \bar{\nu}_{\tau} P_+ \tau H^+ + \text{H.c.} \right\},
\end{aligned} \tag{7}$$

which are different according to the 2HDM type. In this work, we focus on type I. To facilitate the discussion below, we will call the type I with the conditions of Eq. (4) the inverted type I. Then the Higgs coupling modifiers are

$$\xi_f^H = 1, \quad \xi_{t,b,\tau}^h = \frac{1}{t_\beta}, \quad \xi_t^A = -\xi_{b,\tau}^A = \frac{1}{t_\beta}. \quad (8)$$

The trilinear Higgs couplings as dimensionless parameters are defined by

$$\begin{aligned} \mathcal{L}_{\text{tri}} = \sum_{\varphi_0=h,H} v \left\{ \frac{1}{3!} \hat{\lambda}_{\varphi_0\varphi_0\varphi_0} \varphi_0^3 + \frac{1}{2} \hat{\lambda}_{\varphi_0AA} \varphi_0 A^2 + \lambda_{\varphi_0H^+H^-} \varphi_0 H^+ H^- \right\} \\ + \frac{1}{2} \hat{\lambda}_{Hhh} v H h^2 + \frac{1}{2} \hat{\lambda}_{hHH} v h H^2. \end{aligned} \quad (9)$$

In the inverted type I, the couplings are [47, 48]

$$\begin{aligned} \hat{\lambda}_{HHH} &= -\frac{3m_{125}^2}{v^2}, \quad \hat{\lambda}_{hHH} = 0, \\ \hat{\lambda}_{hhh} &= 3\hat{\lambda}_{hAA} = 3\hat{\lambda}_{hH^+H^-} = -\frac{3(M^2 - m_h^2)(t_\beta^2 - 1)}{t_\beta v^2}, \\ \hat{\lambda}_{Hhh} &= -\frac{m_{125}^2 + 2m_h^2 - 2M^2}{v^2}, \\ \hat{\lambda}_{HAA} &= -\frac{m_{125}^2 + 2M_A^2 - 2M^2}{v^2}, \\ \hat{\lambda}_{HH^+H^-} &= -\frac{m_{125}^2 + 2M_{H^\pm}^2 - 2M^2}{v^2}. \end{aligned} \quad (10)$$

The Higgs alignment limit makes the trilinear coupling of the observed Higgs boson  $H$  the same as in the SM,  $\hat{\lambda}_{HHH} \simeq 0.77$ , which is one of the most important targets to measure at the HL-LHC and future colliders [49–54]. Another remarkable feature is that  $\hat{\lambda}_{hhh}$ ,  $\hat{\lambda}_{hAA}$ , and  $\hat{\lambda}_{hH^+H^-}$  have the common factor of  $t_\beta(M^2 - m_h^2)$  in the large  $t_\beta$  limit.

### III. SCANNING AND RGE ANALYSIS

Before studying the high-energy behavior of the model via RGE, the preparation of the allowed parameter points at the electroweak scale is an essential prerequisite. Therefore, we randomly scan five model parameters in the range of

$$\begin{aligned} t_\beta \in [1, 50], \quad M_A \in [10, 3000] \text{ GeV}, \quad m_{12}^2 \in [-3000^2, 3000^2] \text{ GeV}^2, \\ M_{H^\pm} \in [80, 3000] \text{ GeV}, \quad m_h \in [10, 120] \text{ GeV}, \end{aligned} \quad (11)$$

and cumulatively impose the following constraints:

- **Theoretical requirements**

We demand the bounded-from-below Higgs potential [55], tree-level unitarity of scalar-scalar scatterings [41, 56–58], perturbativity [39], and the stability of the  $CP$ -conserving

vacuum with  $v = 246$  GeV [59–61]. We use the public code 2HDMC-v1.8.0 [62]. For the perturbativity, 2HDMC requires that the magnitudes of all the quartic couplings among physical Higgs bosons be less than  $4\pi$ . However, 2HDMC does not check whether our vacuum is the global minimum of the potential. We demand the tree-level vacuum stability condition of [61]

$$m_{12}^2 (m_{11}^2 - k^2 m_{22}^2) (t_\beta - k) > 0, \quad (12)$$

where  $k = (\lambda_1/\lambda_2)^{1/4}$ . The tree-level conditions have been known to be more than sufficient up to very high scales in the Higgs alignment limit [30, 63].

- **Peskin-Takeuchi oblique parameters** [64]

The oblique parameters of  $S$ ,  $T$ , and  $U$  in the 2HDM [65–67] should satisfy the current best-fit results at 95% C.L. [68]:

$$\begin{aligned} S &= -0.02 \pm 0.10, \\ T &= 0.03 \pm 0.12, \quad U = 0.01 \pm 0.11, \\ \rho_{ST} &= 0.92, \quad \rho_{SU} = -0.80, \quad \rho_{TU} = -0.93, \end{aligned} \quad (13)$$

where  $\rho_{ij}$  is the correlation matrix.

- **Flavor changing neutral currents**

We demand that the most recent observables from  $B$  physics be satisfied at 95% C.L. [69–71]. We adopt the results of Ref. [69].

- **Higgs precision data**

We use the public code HIGGSIGNALS-v2.6.2 [72] to check the consistency with the Higgs precision data. Based on the  $\chi^2$  value for 111 Higgs observables [73–80] with five parameters, we require that the  $p$ -value be larger than 0.05.

- **Direct search bounds**

We demand that the model prediction to the cross sections of the direct search modes for new scalar bosons at the LEP, Tevatron, and LHC should be less than 95% C.L. upper bound on the observed cross sections. The open code HIGGSBOUNDS-v5.10.2 [81] is used.

Brief comments on the recent CDF measurement of the  $W$ -boson mass [82],  $m_W^{\text{CDF}} = 80.4335 \pm 0.0094$  GeV, are in order here. If we accept  $m_W^{\text{CDF}}$ , the oblique parameters change into  $S_{\text{CDF}} = 0.15 \pm 0.08$  and  $T_{\text{CDF}} = 0.27 \pm 0.06$  with  $U = 0$  [83]. Although  $m_W^{\text{CDF}}$  has important implications on the 2HDM [35, 36, 83–96], our main conclusion on the role of trilinear Higgs couplings in disentangling the high- and low-cutoff scales does not change. Therefore, we focus on the oblique parameters without the CDF  $m_W$  measurement.

Over the parameter points that pass the above constraints, we evolve the following parameters via the RGE, by using the public code 2HDME [32, 97]:

$$g_{1,2,3}, \quad \lambda_{1,\dots,5}, \quad \xi_f^{h,H,A}, \quad m_{11}, \quad m_{12}, \quad m_{22}^2, \quad v_{1,2}. \quad (14)$$

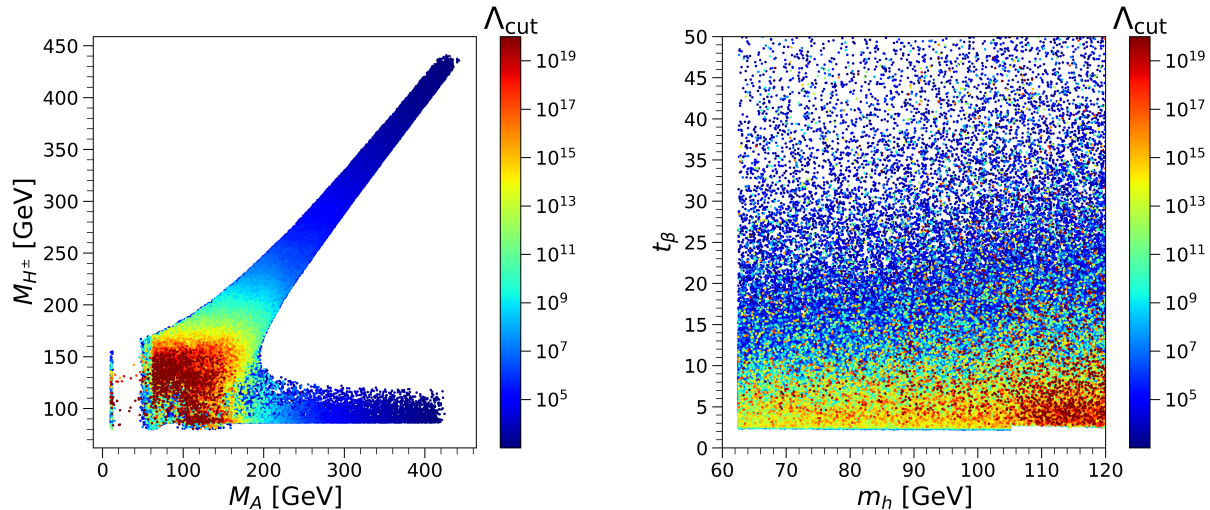


FIG. 2:  $M_{H^\pm}$  versus  $M_A$  in the left panel and  $t_\beta$  versus  $m_h$  in the right panel. The color code denotes the cutoff scale  $\Lambda_{\text{cut}}$ .

We include the mixing effects of two scalar doublet fields (with equal quantum numbers) on  $v_1$  and  $v_2$ , which bring about the RG running of  $t_\beta$ . The top quark pole mass scale,  $m_t^{\text{pole}} = 173.4$  GeV, is used to match the 2HDM to the SM. The boundary conditions at  $m_t^{\text{pole}}$  are referred to Ref. [32]. The  $\beta$  functions of the gauge, Yukawa, and quartic couplings at one loop level are presented in Appendix A. Since the difference between the one-loop and two-loop RG running is not large,<sup>2</sup> we take the one-loop RGE to efficiently cover all the parameter points.

Now let us describe how we obtained the cutoff scale  $\Lambda_{\text{cut}}$ . For each parameter point, we perform the RGE evolution up to the next high energy scale<sup>3</sup> and check three conditions, tree-level unitarity, perturbativity, and vacuum stability.<sup>4</sup> If all three are satisfied, we increase the energy scale into the next step. If any condition is violated, we stop the running and record the energy scale as  $\Lambda_{\text{cut}}$ . We find that the Landau pole appears at a higher scale than  $\Lambda_{\text{cut}}$ . We additionally require that the cutoff scale should be larger than 1 TeV. In what follows, the “viable parameter points” denote the parameter points that satisfy the aforementioned constraints and  $\Lambda_{\text{cut}} > 1$  TeV.

Strong correlations exist between the cutoff scale and the model parameters. In Fig. 2, we present the viable parameter points over the plane of  $(M_A, M_{H^\pm})$  in the left panel and  $(m_h, t_\beta)$  in the right panel. The color code denotes the cutoff scale  $\Lambda_{\text{cut}}$ . We sorted the parameter points according to  $\Lambda_{\text{cut}}$ , and stacked them in order of  $\Lambda_{\text{cut}}$ , the points with low  $\Lambda_{\text{cut}}$  underneath and those with high  $\Lambda_{\text{cut}}$  on top. The overlap is due to the projection of five-dimensional parameter

<sup>2</sup> For randomly selected parameter points, we compared  $\Lambda_{\text{cut}}$  at one-loop level with  $\Lambda_{\text{cut}}$  at two-loop level. The difference is  $\mathcal{O}(10)\%$ .

<sup>3</sup> To cover from the electroweak scale to the Planck scale, we take a uniform step in  $\log(Q)$ .

<sup>4</sup> Note that 2HDMs use the perturbativity condition of  $|\lambda_{1,\dots,5}| < 4\pi$  and the tree-level vacuum stability conditions in Refs. [55, 98].



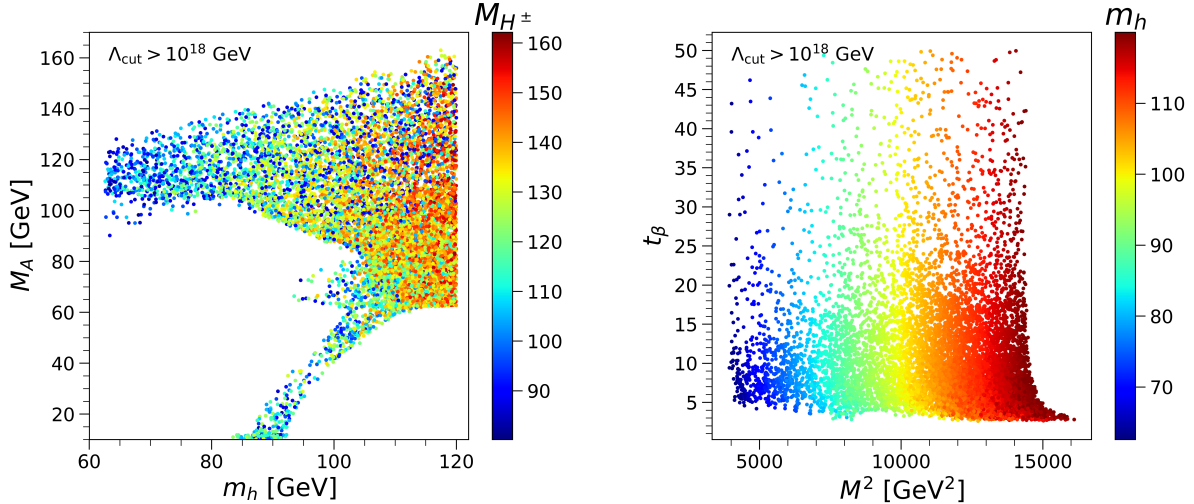


FIG. 3: For  $\Lambda_{\text{cut}} > 10^{18}$  GeV,  $M_A$  versus  $m_h$  in the left panel and  $t_\beta$  versus  $M^2$  in the right panel. The color code denotes  $M_{H^\pm}$  in the left panel and  $m_h$  in the right panel.

space in Eq. (5) on a two-dimensional subspace.

Several remarkable features are shown in Fig. 2. First, the viable parameter points are pretty limited even with the weak condition of  $\Lambda_{\text{cut}} > 1$  TeV. The upper bounds on  $M_A$  and  $M_{H^\pm}$  exist as  $M_A, M_{H^\pm} \lesssim 430$  GeV, to which the condition of  $\Lambda_{\text{cut}} > 1$  TeV plays a critical role. The Peskin-Takeuchi oblique parameter  $T$  is satisfied if  $M_{H^\pm} \sim M_A$  or  $M_{H^\pm} \sim m_h$ , which explains two branches in the left panel of Fig. 2. The lower branch corresponds to  $M_{H^\pm} \sim m_h$ , which puts the upper bound on the charged Higgs boson mass. For the intermediate mass range of  $M_A, M_{H^\pm} \lesssim 200$  GeV, there is no particular correlation between  $M_A$  and  $M_{H^\pm}$ . However, meaningful correlations appear outside the box with  $M_A, M_{H^\pm} \lesssim 200$  GeV. If  $M_{H^\pm} \gtrsim 200$  GeV (belonging to the upper branch),  $M_{H^\pm} \simeq M_A$ . If  $M_{H^\pm} \lesssim 200$  GeV and  $M_A \gtrsim 200$  GeV (belonging to the lower branch),  $M_{H^\pm} \sim 100$  GeV. The lighter  $CP$ -even Higgs boson mass  $m_h$  (right panel of Fig. 2) is heavier than half the observed Higgs boson mass due to the strong constraint from the exotic Higgs boson decay of  $H \rightarrow hh$ . For  $t_\beta$ , most values in the scanning are permitted. Although the density of the allowed  $t_\beta$  in the scatter plot is lower for larger  $t_\beta$ , we cannot conclude that large  $t_\beta$  is disfavored: nature chooses just one parameter point.

The second remarkable feature of Fig. 2 is that substantial parameter points in the inverted type I remain stable all the way up to the Planck scale. Let us investigate the characteristics of the parameter points with the high-cutoff scale. In Fig. 3, we show  $M_A$  versus  $m_h$  (left panel) and  $t_\beta$  versus  $M^2$  (right panel) after imposing  $\Lambda_{\text{cut}} > 10^{18}$  GeV. The color code in the left (right) panel denotes  $M_{H^\pm}$  ( $m_h$ ). It is clearly seen that the high-cutoff scale requires *light* masses of the extra Higgs bosons like  $M_A, M_{H^\pm} \lesssim 160$  GeV. We observe that the charged Higgs boson is lighter than the top quark for the Planck-scale cutoff. However, the lower bounds of  $M_A \gtrsim 10$  GeV,  $m_h \gtrsim 62.5$  GeV, and  $M_{H^\pm} \gtrsim 80$  GeV do not change by imposing  $\Lambda_{\text{cut}} > 10^{18}$  GeV. Similarly, the Planck-scale cutoff does not affect the values of  $t_\beta$ , as shown

in the right panel of Fig. 3.

The values of  $M^2$  are also limited even with  $\Lambda_{\text{cut}} > 1$  TeV. Only the positive values of  $M^2$  are permitted because negative  $M^2$  enhances  $\lambda_1$  through the terms proportional to  $t_\beta^2$ . Large  $\lambda_1$  at the electroweak scale quickly evolves into an unacceptably large value, which endangers the global minimum condition of the vacuum [59–61]. For  $\Lambda_{\text{cut}} > 10^{18}$  GeV, a unique correlation of  $M^2 \simeq m_h^2$  appears as shown in the right panel in Fig. 3. It is also ascribed to the  $t_\beta^2$  terms in  $\lambda_1$ . The condition of  $M^2 \simeq m_h^2$  suppresses the  $t_\beta^2$  terms and thus helps to retain the stability of the scalar potential.

Although the high-cutoff scale demands light masses of the extra Higgs bosons, the inverse is not true. All the mass spectra in the left panel of Fig. 3 also accommodate a low-cutoff scale: see Fig. 1. Even if we observe  $m_h = M_A = 100$  GeV and  $M_{H^\pm} = 140$  GeV, for example, the mass spectrum alone cannot tell whether the cutoff scale is high or low. The reader may suggest to use  $t_\beta$  as a discriminator of the cutoff scale. However, measuring  $t_\beta$  in type I is challenging at the LHC, especially when  $t_\beta \gg 1$ . The value of  $t_\beta$  governs the fermionic productions (from the top quark decay or gluon fusion via quark loops) and fermionic decays of the extra Higgs bosons. If  $t_\beta$  is large, the fermionic production of the extra Higgs bosons is highly suppressed because all the Yukawa couplings of the extra Higgs bosons are inversely proportional to  $t_\beta$  in type I. The bosonic productions such as  $q\bar{q} \rightarrow Z^* \rightarrow Ah$  and  $q\bar{q} \rightarrow W^* \rightarrow H^\pm h/A$  [37, 99–109] do not give information about  $t_\beta$ . Moreover, the fermionic decay parts are insensitive to  $t_\beta$  because of the same dependence of all the Yukawa couplings on  $t_\beta$ . If we cannot measure the exact value of large  $t_\beta$ , it is reasonable to include all the viable parameter points with  $t_\beta > 10$  when pursuing a way to discriminate the high and low  $\Lambda_{\text{cut}}$ .

#### IV. TRILINEAR HIGGS COUPLINGS

In this section, we study the trilinear Higgs couplings to measure  $\Lambda_{\text{cut}}$ . We consider the following three benchmark points:

$$\begin{aligned}
\text{BP-1:} \quad & m_h = 70 \text{ GeV}, & M_A = 110 \text{ GeV}, & M_{H^\pm} = 110 \text{ GeV}, & (15) \\
\text{BP-2:} \quad & m_h = 100 \text{ GeV}, & M_A = 100 \text{ GeV}, & M_{H^\pm} = 140 \text{ GeV}, \\
\text{BP-3:} \quad & m_h = 110 \text{ GeV}, & M_A = 70 \text{ GeV}, & M_{H^\pm} = 140 \text{ GeV},
\end{aligned}$$

all of which accommodate the cutoff scale from 1 TeV to  $10^{19}$  GeV. As discussed in the previous section, we focus on the large  $t_\beta$  limit as

$$\text{Large } t_\beta \text{ case: } t_\beta > 10. \quad (16)$$

For  $m_{12}^2$ , we incorporate all the values that satisfy the constraints in Sec. III.

Let us turn into the trilinear Higgs couplings versus  $\Lambda_{\text{cut}}$ . In Fig. 4, we present  $\hat{\lambda}_{hhh}$  (left panel),  $\hat{\lambda}_{Hhh}$  (middle panel), and  $\hat{\lambda}_{HHH}$  (right panel) at the electroweak scale, as a function of  $\Lambda_{\text{cut}}$ : note that  $\hat{\lambda}_{hAA} = \hat{\lambda}_{hH^+H^-} = \hat{\lambda}_{hhh}/3$ . Here only the BP-2 results are shown because

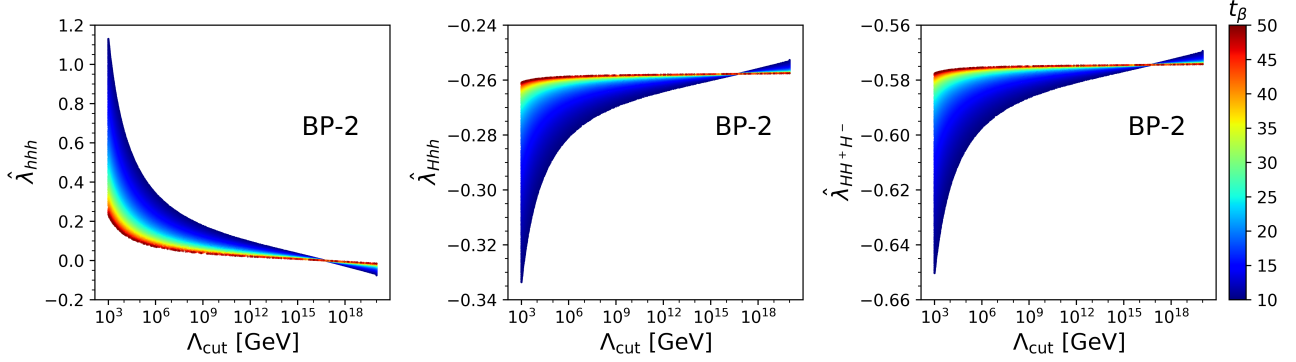


FIG. 4: Trilinear Higgs couplings of  $\hat{\lambda}_{hhh}$  (left panel),  $\hat{\lambda}_{Hhh}$  (middle panel), and  $\hat{\lambda}_{HH+H-}$  (right panel) against the cutoff scale  $\Lambda_{\text{cut}}$ . The color code denotes  $t_\beta$ . We take BP-2 where  $m_h = M_A = 100$  GeV,  $M_{H^\pm} = 140$  GeV, and  $t_\beta > 10$ .

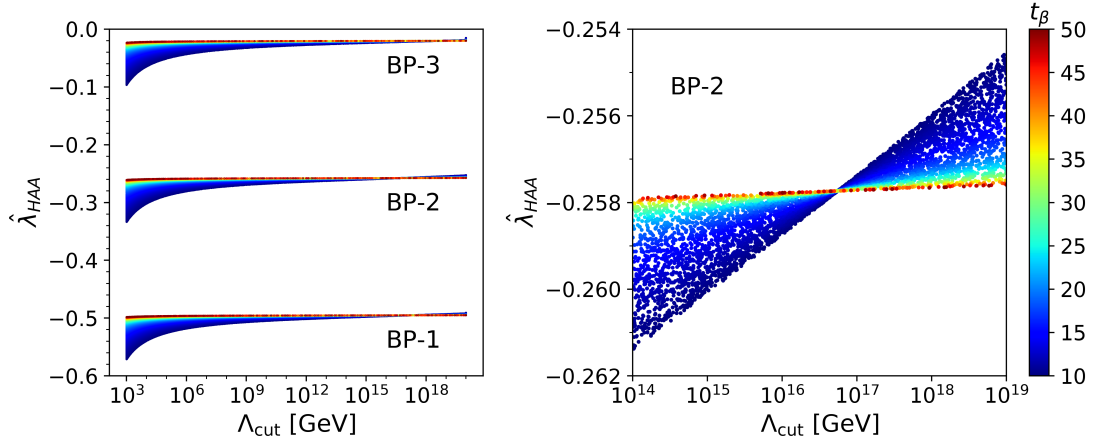


FIG. 5: Trilinear Higgs couplings of  $\hat{\lambda}_{HAA}$  versus the cutoff scale  $\Lambda_{\text{cut}}$  for BP-1, BP-2, and BP-3 (left panel) and  $\hat{\lambda}_{HAA}$  around the *focus* cutoff scale for BP-2 (right panel). The color code denotes  $t_\beta$ . We include all the viable parameter points with  $t_\beta > 10$ .

BP-1 and BP-3 yield similar results with  $\mathcal{O}(10)\%$  differences. The value of  $t_\beta$  is shown via the color code. It is impressive that the values of  $\hat{\lambda}_{hhh}$ ,  $\hat{\lambda}_{Hhh}$ , and  $\hat{\lambda}_{HH+H-}$  for  $\Lambda_{\text{cut}} = 10^{18}$  are not overlapped with those for  $\Lambda_{\text{cut}} \lesssim 10^{17}$  GeV, although the allowed values for lower  $\Lambda_{\text{cut}}$  are considerably spread by the unfixed  $t_\beta$  and  $m_{12}^2$ . The most sensitive dependence on  $\Lambda_{\text{cut}}$  is shown in  $\hat{\lambda}_{hhh}$ , which ranges in  $[-0.09, 1.1]$ . Since  $\hat{\lambda}_{hhh} = 0$  is included, the change of  $\hat{\lambda}_{hhh}$  according to  $\Lambda_{\text{cut}}$  is huge. On the other hand, the variations of  $\hat{\lambda}_{Hhh}$  and  $\hat{\lambda}_{HH+H-}$  are small within  $10\% \sim 20\%$ .

In the left panel of Fig. 5, we present  $\hat{\lambda}_{HAA}$  versus  $\Lambda_{\text{cut}}$  for BP-1, BP-2, and BP-3. Unlike  $\hat{\lambda}_{hhh}$ ,  $\hat{\lambda}_{Hhh}$ , and  $\hat{\lambda}_{HH+H-}$ , the value of  $\hat{\lambda}_{HAA}$  is sensitive to the benchmark point. For high  $\Lambda_{\text{cut}}$ ,  $|\hat{\lambda}_{HAA}|$  of BP-1 is about 25 times larger than that of BP-3.  $\hat{\lambda}_{HAA}$  depends on  $M_A$  and  $M^2$ , not on  $t_\beta$ . Since  $M^2 \approx m_h^2$  and  $m_h \sim m_{125}$  as shown in Fig. 3, the  $M^2$  contribution to  $\hat{\lambda}_{HAA}$  is nearly cancelled by the  $m_{125}$  contribution. So, the heavier  $M_A$  is, the larger  $|\hat{\lambda}_{HAA}|$  is.

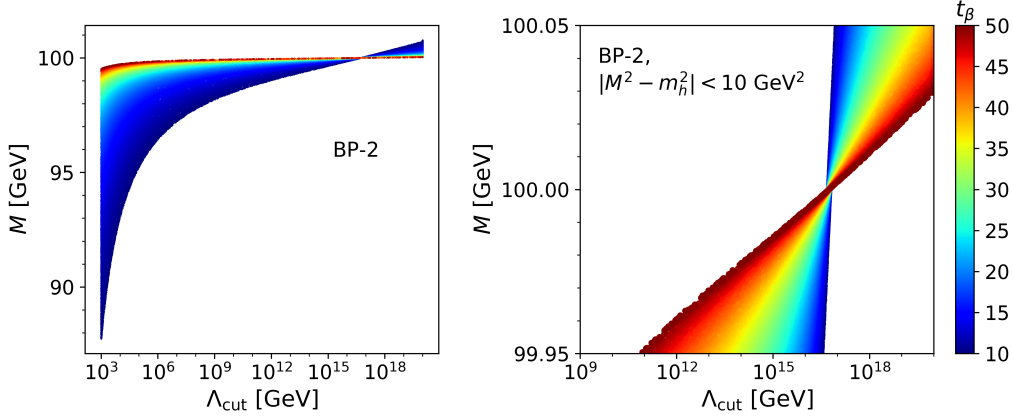


FIG. 6:  $M(\equiv \sqrt{M^2})$  versus the cutoff scale  $\Lambda_{\text{cut}}$  for BP-2 with the color code of  $t_\beta$ . The left panel presents the results of all the viable parameter points and the right panel shows those with  $|M^2 - m_h^2| \leq 10 \text{ GeV}^2$ .

We observe a special  $\Lambda_{\text{cut}}$  in Fig. 4 and the right panel of Fig. 5. Around  $\Lambda_{\text{cut}} \simeq 10^{17} \text{ GeV}$ , all the trilinear Higgs couplings are almost fixed. Even though we present only the results of BP-2 in Fig. 4, the same behavior is found in BP-1 and BP-3. The spread trilinear Higgs couplings are focused on a single cutoff point which we call  $\Lambda_{\text{cut}}^{\text{focus}}$ . Since the allowed value of  $M^2$  plays a crucial role in understanding  $\Lambda_{\text{cut}}^{\text{focus}}$ , we show  $M(\equiv \sqrt{M^2})$  versus the cutoff scale  $\Lambda_{\text{cut}}$  for BP-2 in Fig. 6. The left panel presents the results of all the viable parameter points. It is clear to see that the parameter points with  $\Lambda_{\text{cut}} = \Lambda_{\text{cut}}^{\text{focus}}$  satisfy the condition of  $M^2 = m_h^2$ . We found that the reverse holds true. If we allow small deviation like  $|M^2 - m_h^2| \leq 10 \text{ GeV}^2$  as in the right panel of Fig. 6, the cutoff scale converges to  $\Lambda_{\text{cut}} = \Lambda_{\text{cut}}^{\text{focus}}$  for  $t_\beta = 10$  but ranges from  $10^{12} \text{ GeV}$  to the Planck scale for  $t_\beta = 50$ . Then why does the condition of  $M^2 = m_h^2$  fix the trilinear Higgs coupling? It is because the condition removes the  $t_\beta$  dependence of the trilinear couplings, which is the main source for their variation. In addition,  $M^2 = m_h^2$  removes the dangerous  $t_\beta^2$  terms of  $\hat{\lambda}_1$ , which guarantees the high-energy scale of  $\Lambda_{\text{cut}}^{\text{focus}}$ .

Now we discuss the other 2HDM scenarios. This paper concentrates on the inverted type I in the Higgs alignment limit. Let us first consider a small deviation from the alignment. Since the Higgs precision prospect at the future muon collider associated with the HL-LHC and the Higgs factory at  $\sqrt{s} = 250 \text{ GeV}$  is  $\delta\kappa_W \simeq 0.11\%$  [110], we consider two cases of  $|s_{\beta-\alpha}| = 0.05, 0.1$ . In Fig. 7, we present  $\hat{\lambda}_{hhh}$  versus  $\Lambda_{\text{cut}}$  for  $|s_{\beta-\alpha}| = 0.05$  (left panel) and  $|s_{\beta-\alpha}| = 0.1$  (right panel). Here only BP-2 results are shown. For  $|s_{\beta-\alpha}| = 0.05$ , the behavior of  $\hat{\lambda}_{hhh}$  about  $\Lambda_{\text{cut}}$  remains almost same as the alignment case. The values of  $\hat{\lambda}_{hhh}$  for  $\Lambda_{\text{cut}} = 10^{18} \text{ GeV}$  are not overlapped with those for  $\Lambda_{\text{cut}} \lesssim 10^6 \text{ GeV}$ . If we increase the deviation from the alignment into  $|s_{\beta-\alpha}| = 0.1$ , the band of  $\hat{\lambda}_{hhh}$  widens. The values of  $\hat{\lambda}_{hhh}$  for  $\Lambda_{\text{cut}} = 10^{18} \text{ GeV}$  are mostly overlapped with the low cutoff scale, except for  $\Lambda_{\text{cut}} \lesssim 10 \text{ TeV}$ .

Finally, we discuss whether we have similar results for other types or the normal Higgs scenario where the lighter  $CP$ -even Higgs boson is the observed one. In the inverted Higgs

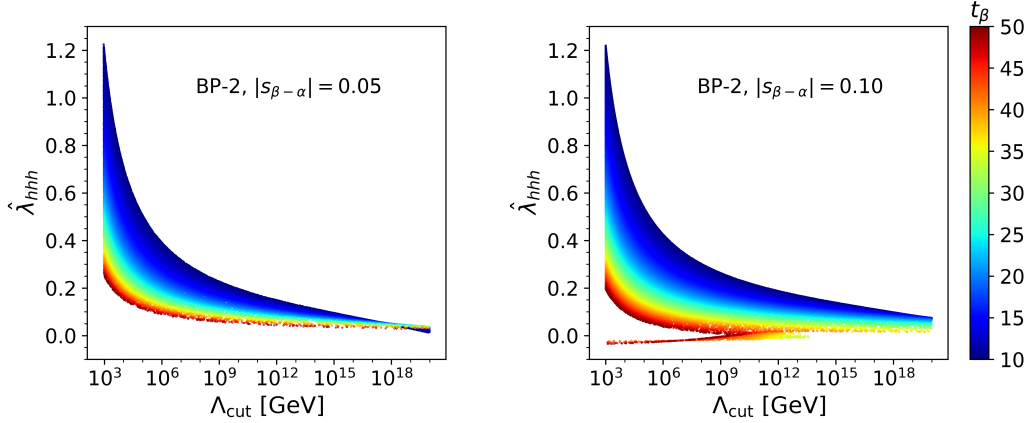


FIG. 7: For the small deviation from the Higgs alignment limit,  $\hat{\lambda}_{hhh}$  versus the cutoff scale  $\Lambda_{\text{cut}}$  for BP-2 with the color code of  $t_\beta$ . The left (right) panel presents the results of  $|s_{\beta-\alpha}| = 0.05$  ( $|s_{\beta-\alpha}| = 0.1$ ).

scenario, type II and type Y are excluded by imposing the condition of  $\Lambda_{\text{cut}} > 1$  TeV [35] because the constraint from  $b \rightarrow s\gamma$ ,  $M_{H^\pm} > 800$  GeV [111], contradicts the required light masses of the BSM Higgs bosons. Type X in the inverted scenario can accommodate  $\Lambda_{\text{cut}} = 10^{18}$  GeV and show similar behaviors of the trilinear Higgs couplings about the cutoff scales. In the normal scenario, all four types can retain the theoretical stability up to  $\Lambda_{\text{cut}} = 10^{18}$  GeV. The high cutoff scale demands the almost exact mass degeneracy among the BSM Higgs boson masses, i.e.,  $M = M_A = M_H = M_{H^\pm}$ , but does not put any upper bounds on the masses. So, the question for the normal scenario is changed: how can we distinguish the high- and low-cutoff scales via observables *if we observe a highly degenerate mass spectrum of the extra Higgs bosons*? It is more challenging than in the inverted scenario due to the heavy masses and the soft decay products of the BSM Higgs bosons. Nevertheless, the similar behavior of  $\hat{\lambda}_{HHH}$  about  $\Lambda_{\text{cut}}$  leaves a motivation for the phenomenological study in future colliders.

## V. LHC PHENOMENOLOGY

For the LHC phenomenology, we first present the branching ratios of  $h$  (left panels),  $A$  (middle panels), and  $H^\pm$  (right panels) as a function of  $\Lambda_{\text{cut}}$  in Fig. 8. The results of BP-1, BP-2, and BP-3 are in the upper, middle, and lower panels, respectively. We include all the viable parameter points. The first noteworthy feature in Fig. 8 is that the dominant decay mode of the extra Higgs boson with the given mass spectra is insensitive to the cutoff scale, even though the two parameters of  $t_\beta (> 10)$  and  $m_{12}^2$  are not fixed. The decay of  $h$  depends on the hierarchy between  $m_h$  and  $M_A$ . When  $m_h \leq M_A$  as in BP-1 and BP-2, the leading (next-to-leading) decay mode is  $h \rightarrow bb$  ( $h \rightarrow \tau^+\tau^-$ ). However, if  $m_h > M_A$  as in BP-3, the dominant decay mode is  $h \rightarrow AZ^*$ . The suppressed Yukawa couplings of  $h$  by large  $t_\beta$  enhance the bosonic decays modes if kinematically open. The decay of  $A$  is primarily determined by

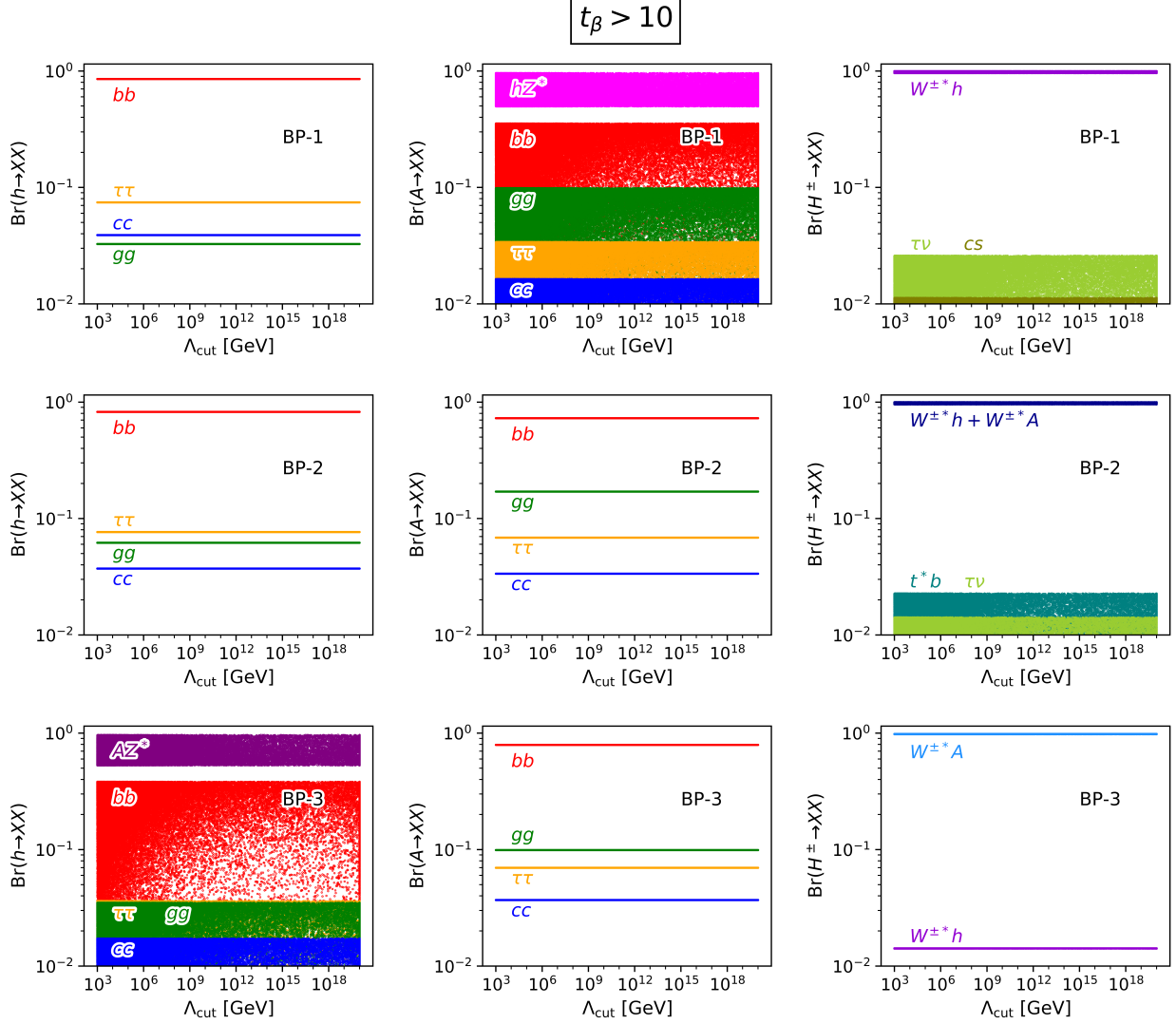


FIG. 8: Branching ratios of  $h$  (upper panels),  $A$  (middle panels), and  $H^\pm$  (lower panels) about the cutoff scale  $\Lambda_{\text{cut}}$ . All the viable parameter points with  $t_\beta > 10$  are included.

the hierarchy between  $M_A$  and  $m_h$ . For BP-2 and BP-3 with  $M_A \leq m_h$ , the pseudoscalar  $A$  dominantly decays into a pair of  $b$  quarks with  $\text{Br}(A \rightarrow b\bar{b}) \gtrsim 0.73$ . The next-to-leading decay mode of  $A$  is into  $gg$ . The substantial  $\text{Br}(A \rightarrow gg)$  is attributed to the larger loop amplitudes of a pseudoscalar than those of a scalar for the spin-1/2 particle contributions [112]. The third one is  $A \rightarrow \tau^+\tau^-$ . If  $M_A > m_h$  as in BP-1, however,  $\text{Br}(A \rightarrow hZ^*)$  becomes the largest, which holds for the entire range of  $\Lambda_{\text{cut}}$ . The decay into  $b\bar{b}$  is mostly next-to-leading.<sup>5</sup>

The charged Higgs boson mainly decays into  $hW^{\pm*}$  and  $AW^{\pm*}$ , for the three benchmark points. Once kinematically allowed, the bosonic decay modes are dominant: the  $H^\pm$ - $W^\mp$ - $h$  vertex is proportional to  $c_{\beta-\alpha}$  ( $= 1$ ); the  $H^\pm$ - $W^\mp$ - $A$  vertex is originated from the pure gauge

<sup>5</sup> We caution the reader that the scattered points are overlapped except for the leading decay mode. For some parameter points,  $A \rightarrow gg$  can be next-to-leading.

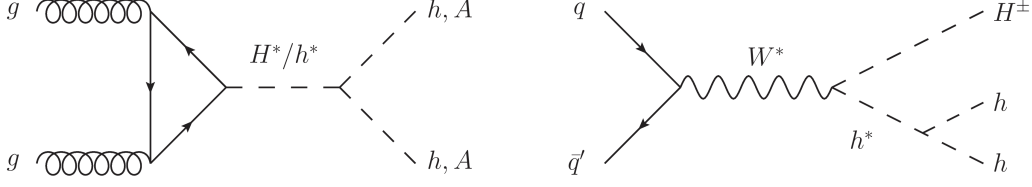


FIG. 9: Feynman diagrams of  $gg \rightarrow hh/AA$  (left panel) and  $q\bar{q}' \rightarrow W^* \rightarrow H^\pm hh$  (right panel).

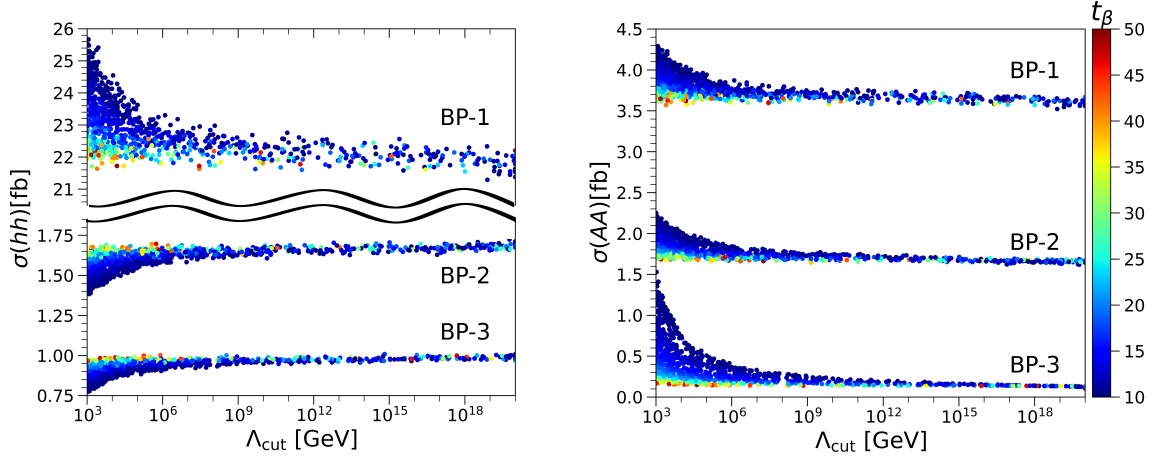


FIG. 10: Cross sections of  $gg \rightarrow hh$  (left panel) and  $gg \rightarrow AA$  (right panel) at the 14 TeV LHC, as a function of  $\Lambda_{\text{cut}}$ . The color code denotes  $t_\beta$ . The description of the benchmarks is in the main text.

interaction. In BP-3 with  $M_{H^\pm} > M_A$  and  $M_{H^\pm} > m_h$ , the branching ratios of the fermionic modes are below 1%. If either  $m_h$  or  $M_A$  is beyond the kinematic threshold as in BP-1 and BP-2, the fermionic decay modes become considerable. The leading fermionic decay mode depends on the charged Higgs bosons mass. For BP-1 where  $M_{H^\pm}$  is substantially lighter than the top quark mass,  $H^\pm \rightarrow \tau\nu$  has the largest branching ratio among the fermionic decay modes, followed by  $H^\pm \rightarrow cs$ . In BP-2 where  $M_{H^\pm}$  is near to the top quark mass,  $H^\pm \rightarrow t^*b$  becomes the leading fermionic mode, followed by  $H^\pm \rightarrow \tau\nu$ .

To probe the trilinear Higgs couplings at the LHC, we need to consider multi-Higgs production mediated by Higgs bosons. The first important are the di-Higgs processes,  $gg \rightarrow H/h \rightarrow hh/AA$ . The corresponding Feynman diagram<sup>6</sup> is in the left panel of Fig. 9. The contribution of  $H$  destructively interferes with that of  $h$  because the sign of  $\hat{\lambda}_{Hhh}$  and  $\hat{\lambda}_{hhh}$  are opposite to each other: see Fig. 4.

In Fig. 10, we present as a function of  $\Lambda_{\text{cut}}$  the parton-level production cross sections for  $gg \rightarrow hh$  (left panel) and  $gg \rightarrow AA$  (right panel) at the 14 TeV LHC over the viable parameter points. All the three benchmark points in Eq. (15) are considered. The color code denotes  $t_\beta$ . To calculate the parton-level cross sections, we first obtained the Universal Feyn-

<sup>6</sup> We omit the box diagrams from the top quark loop because two factors of  $1/t_\beta$  suppress them.

Rules Output (UFO) [113] by using FEYNRULES [114]. Then we interfered the UFO file with MADGRAPH5-AMC@NLO [115] and calculated the cross sections at the 14 TeV LHC with the NNPDF31\_LO\_AS\_0118 parton distribution function set [116].

For the production cross sections of  $gg \rightarrow hh$ , the most crucial factor is  $m_h$ . The lighter  $m_h$  is, the larger  $\sigma(gg \rightarrow hh)$  is. BP-1 yields the largest cross section. On the contrary, the production cross section of  $gg \rightarrow AA$  is larger for heavier  $M_A$ . The BP-1, which has the heaviest  $M_A$  among the three benchmark points, has the largest cross section. It seems contradictory to the kinematic loss by the heavy  $M_A$ . The main reason is that the dominant contribution to  $gg \rightarrow AA$  is from  $H$  and thus  $\hat{\lambda}_{HAA}$  determines the signal rate. The heavier  $M_A$  is, the larger  $\hat{\lambda}_{HAA}$  is: see Fig. 5.

The dependence of  $\sigma(gg \rightarrow hh/AA)$  on  $\Lambda_{\text{cut}}$  is not large enough to distinct the high- and low-cutoff scales. Even the optimistic case, the process of  $gg \rightarrow hh$  in BP-1 with  $t_\beta = 10$ , makes a few fb difference in the cross sections between  $\Lambda_{\text{cut}} = 1$  TeV and  $\Lambda_{\text{cut}} = 10^{18}$  GeV. It is too small to probe at the HL-LHC with the expected total luminosity of  $3 \text{ ab}^{-1}$ . For larger  $t_\beta$  like 50, the di-Higgs production cross sections become more insensitive to  $\Lambda_{\text{cut}}$ . The weak dependence of  $\sigma(gg \rightarrow hh)$  on  $\Lambda_{\text{cut}}$  is due to the dominant contribution from  $H$  and the destructive interference between the  $H$  and  $h$  contributions. In the BP-1 with  $t_\beta = 10$  and  $\Lambda_{\text{cut}} = 1$  TeV, for example, the cross section from  $H$  alone is  $\sigma(gg \rightarrow H \rightarrow hh) \simeq 36.5$  fb, from  $h$  alone is  $\sigma(gg \rightarrow h \rightarrow hh) \simeq 1.1$  fb, and from the interference  $\sigma(gg \rightarrow hh)_{\text{intf}} \simeq -12.1$  fb. The  $\hat{\lambda}_{Hhh}$  controls the cross section, but its variation about  $\Lambda_{\text{cut}}$  is small.

To single out only one trilinear Higgs coupling, we consider triple Higgs productions at the LHC. Since the gluon fusion production of the tri-Higgs process through the top quark loop is suppressed by large  $t_\beta$ , we concentrate on the tri-Higgs productions mediated by the gauge bosons. Through the  $Z$  boson, we have

$$q\bar{q} \rightarrow Z^* \rightarrow Ah^* \rightarrow Ahh, \quad q\bar{q} \rightarrow Z^* \rightarrow A^*h \rightarrow Ahh, \quad (17)$$

$$q\bar{q} \rightarrow Z^* \rightarrow Ah^* \rightarrow AAA, \quad (18)$$

and through  $W$

$$q\bar{q}' \rightarrow W^* \rightarrow H^\pm h^* \rightarrow H^\pm hh, \quad (19)$$

$$q\bar{q}' \rightarrow W^* \rightarrow H^\pm h^* \rightarrow H^\pm AA, \quad (20)$$

$$q\bar{q}' \rightarrow W^* \rightarrow H^\pm A^* \rightarrow H^\pm Ah. \quad (21)$$

As a representative, we present the Feynman diagram of  $q\bar{q}' \rightarrow H^\pm hh$  in the right panel of Fig. 9. Since all the above processes in Eqs. (17)–(21) have the same topology of the Feynman diagram, the production cross sections as a function of  $\Lambda_{\text{cut}}$  show almost the same behavior. In BP-2, for example,  $\sigma(pp \rightarrow Ahh)/\sigma(pp \rightarrow H^\pm hh) \simeq 0.9$  holds for all  $\Lambda_{\text{cut}}$ .

In Fig. 11, we present the parton-level production cross sections of  $q\bar{q}' \rightarrow H^\pm hh$  at the 14 TeV LHC for BP-1 (left panel), BP-2 (middle panel), and BP-3 (right panel). The color code denotes  $t_\beta$ . The difference of the cross section according to  $\Lambda_{\text{cut}}$  is big enough to distinguish the



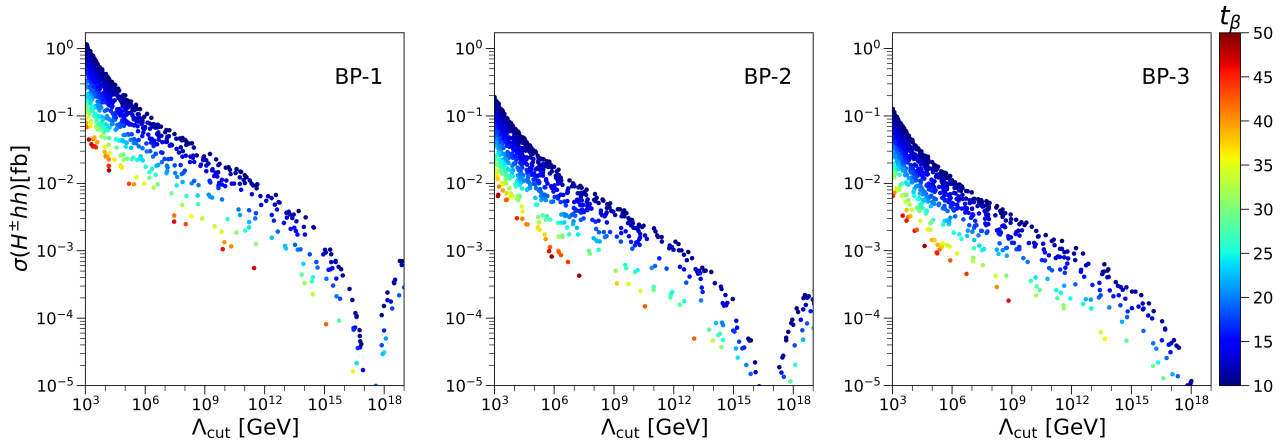


FIG. 11: Cross sections of  $q\bar{q}' \rightarrow H^\pm hh$  at the 14 TeV LHC as a function of  $\Lambda_{\text{cut}}$ , for BP-1 (left), BP-2 (middle), and BP-3 (right). The color codes indicate  $t_\beta$ .

high- and low-cutoff scales of the inverted type I. The ratio of the cross section for  $\Lambda_{\text{cut}} = 1$  TeV to that for  $\Lambda_{\text{cut}} = 10^{18}$  GeV is more than about  $10^3$ . This is the most remarkable result of our study. Measuring the signal rate of the triple Higgs production tells whether the cutoff scale is high or low.

Finally, we discuss the discovery potential at the HL-LHC. Discriminating the high- and low-cutoff scales through  $gg \rightarrow hh/AA$  requires the precision measurement on the cross section within  $\sim 1$  fb. Let us roughly estimate the feasibility. The processes of  $gg \rightarrow hh$  and  $gg \rightarrow AA$  mainly yield  $4b$  final states because  $A/h \rightarrow bb$  is leading or next-to-leading. Resembling the di-Higgs process in the SM, they are challenging to observe for two reasons. First, the cross section itself is too small. The maximum cross section, which happens for  $\Lambda_{\text{cut}} = 1$  TeV, reaches  $\mathcal{O}(10)$  fb. It is to be compared with the SM leading order result of  $\sigma(gg \rightarrow h_{\text{SM}} h_{\text{SM}})_{\text{LO}} \simeq 17$  fb at  $\sqrt{s} = 14$  TeV [117]. Since the projected signal significance of the SM Higgs boson pair production at the HL-LHC with the total luminosity of  $3 \text{ ab}^{-1}$  is  $3.0\sigma$ , when the  $bbbb$ ,  $bb\tau^+\tau^-$ , and  $bb\gamma\gamma$  decay channels are all combined [118], it is hard to observe  $gg \rightarrow hh/AA$ . The second difficulty comes from the softer  $b$  jets than in the SM di-Higgs process. For  $gg \rightarrow hh \rightarrow 4b$ , the lighter  $m_h$  than 125 GeV yields soft  $b$  quarks. For  $gg \rightarrow AA \rightarrow 4b$ , most of the viable parameter points in Fig. 3 have  $M_A < 125$  GeV, which generate soft  $b$  quarks. As the  $b$  tagging efficiency is reduced, the signal significance decreases as well. In summary, the di-Higgs process is not efficient to probe the cutoff scale.

The triple Higgs production of  $H^\pm hh$  has higher discovery potential. Since the charged Higgs boson mainly decays into  $W^\pm A/h$  in the three benchmark points, followed by  $h/A \rightarrow bb$ , the final state is  $6b + \ell\nu$ . This attractive channel has not been studied in the literature.<sup>7</sup> The main

<sup>7</sup> The final state of  $4j + \ell\nu$  was studied for the vector boson scattering of  $WW \rightarrow WW$  [119], and the SM Higgs boson decaying into a fat jet consisting of  $4b/6b/8b$  was studied [120].

backgrounds are

$$\begin{aligned}
t + \bar{t} + \ell\nu &\rightarrow bj_b^{\text{mis}} j_b^{\text{mis}} + bj_b^{\text{mis}} j_b^{\text{mis}} + \ell\nu, \\
t + \bar{t} + jj &\rightarrow b\ell\nu + bj_b^{\text{mis}} j_b^{\text{mis}} + j_b^{\text{mis}} j_b^{\text{mis}},
\end{aligned}
\tag{22}$$

where  $j_b^{\text{mis}}$  is the light jet (from  $u, d, s, c,$  and  $g$ ) mistagged as a  $b$  quark jet. We calculated the parton-level cross sections of the backgrounds, with the  $b$  tagging and mistagging efficiencies of  $P_{b\rightarrow b} = 0.7$ ,  $P_{c\rightarrow b} = 0.05$ , and  $P_{j\rightarrow b} = 0.01$ . We imposed the selection cuts of  $p_T^b > 20$  GeV,  $p_T^\ell > 10$  GeV,  $|\eta^{\ell,j}| < 2.5$ ,  $E_T^{\text{miss}} > 20$  GeV, and the separation  $\Delta R_{i'i'} > 0.4$ . After the basic selection, the background cross section from  $t\bar{t}jj$  is about 8.7 ab and from  $t\bar{t}\ell\nu$  is about  $3.8 \times 10^{-4}$  ab. If we impose additional cuts on the invariant mass of two  $b$  jets like  $|m_{bb} - m_h| < 15$  GeV, the backgrounds are negligible. Despite the almost background-free environment, the high  $\Lambda_{\text{cut}}$  yields too small signal rate of  $pp \rightarrow H^\pm hh$  at the 14 TeV LHC.

Exploring the cutoff scale in the inverted type I via the  $6b + \ell\nu$  final state has a better chance in future high-energy colliders such as the Future hadron-hadron Circular Collider (FCC-hh) at CERN [121], the CEPC [122, 123], and the muon collider [124–126]. Particularly, we have high expectations for the muon collider with benchmark energies in the range of  $\sqrt{s} = 3 - 30$  TeV and the integrated luminosity of  $\mathcal{L} = 10(\sqrt{s}/10 \text{ TeV})^2 \text{ ab}^{-1}$ . The triple Higgs processes in Eq. (17) and Eq. (18) with  $q\bar{q}$  replaced by  $\mu^+\mu^-$  will be able to disentangle the high- and low-cutoff scales in the inverted type I.

## VI. CONCLUSION

Beyond the studies on how high the cutoff scale of a new physics model can go up, we have pursued an efficient observable to distinguish the high- and low-cutoff scales. The type I in the 2HDM has been considered for the inverted scenario where the observed Higgs boson at a mass of 125 GeV is the heavier  $CP$ -even Higgs boson  $H$ . We have first obtained the still-available parameter points that satisfy the theoretical requirements, the experimental constraints, and the cutoff scale above 1 TeV. The viable parameter space at the electroweak scale is already limited such that  $M_A, M_{H^\pm} \lesssim 430$  GeV and  $m_h \gtrsim 62.5$  GeV. Through the calculation of the cutoff scale  $\Lambda_{\text{cut}}$  of each viable parameter point by using the RGE, we have shown that the inverted type I can retain the stability all the way up to the Planck scale.

The condition of  $\Lambda_{\text{cut}} > 10^{18}$  GeV requires the light masses of the extra Higgs bosons like  $M_A, M_{H^\pm} \lesssim 160$  GeV. However, the light masses alone cannot guarantee the high-cutoff scale because the parameter points with light masses accommodate  $\Lambda_{\text{cut}}$  from 1 TeV to  $10^{19}$  GeV. Targeting at the phenomenologically challenging case of  $t_\beta > 10$ , we have investigated the trilinear Higgs couplings versus  $\Lambda_{\text{cut}}$ . Although the values of all the trilinear couplings for  $\Lambda_{\text{cut}} = 1$  TeV are different from those for  $\Lambda_{\text{cut}} = 10^{18}$  GeV,  $\hat{\lambda}_{hhh}$  shows a large variation about  $\Lambda_{\text{cut}}$ ,  $\hat{\lambda}_{hhh} \in [-0.09, 1.1]$ . Multi-Higgs boson productions at the LHC have been studied to probe the cutoff scale. The gluon fusion productions of the di-Higgs,  $gg \rightarrow hh/AA$ , are not efficient to measure  $\hat{\lambda}_{hhh}$  because the dominant contribution from  $H$  dilutes the  $h$  contribution. The most

remarkable result is in the tri-Higgs process of  $pp \rightarrow H^\pm hh$  mediated by the  $W$  boson. The signal cross section shows huge variation according to  $\Lambda_{\text{cut}}$ , like  $\sigma_{\Lambda_{\text{cut}}=1 \text{ TeV}}/\sigma_{\Lambda_{\text{cut}}=10^{18} \text{ GeV}} \sim 10^3$ . The precision measurement of  $pp \rightarrow H^\pm hh$  can indeed distinguish the high- and low-cutoff scales of the model. Considering the dominant decay modes of  $H^\pm \rightarrow W^{\pm*}A/h$ ,  $h \rightarrow bb$ , and  $A \rightarrow bb$ , an efficient final state of  $pp \rightarrow H^\pm hh$  is  $6b + \ell\nu$ . Although it enjoys almost background-free environment at the LHC, the small cross section ( $\lesssim 1 \text{ ab}$ ) for  $\Lambda_{\text{cut}} = 10^{18} \text{ GeV}$  motivates future high-energy colliders, especially the muon collider with  $\sqrt{s} = 3 - 30 \text{ TeV}$ .

## Acknowledgments

The work of J. K., S. L, and J. S is supported by the National Research Foundation of Korea, Grant No. NRF-2022R1A2C1007583. S. K. K. was supported by the National Research Foundation of Korea (NRF) grant funded by the Korea government (MSIT) (No.2019R1A2C1088953).

## Appendix A: RGEs in the type I

Focusing on the type I, we present the one-loop level RGEs [26, 30, 41, 127, 128]. The beta functions of gauge couplings are given by

$$16\pi^2\beta_{g_3} = -7g_3^3, \quad (\text{A1})$$

$$16\pi^2\beta_{g_2} = \left(-\frac{10}{3} + \frac{n_d}{6}\right)g_2^3 = -3g_2^3, \quad (\text{A2})$$

$$16\pi^2\beta_{g_1} = \left(\frac{20}{3} + \frac{n_d}{6}\right)g_1^3, \quad (\text{A3})$$

where  $n_d$  is the number of the scalar doublets of the fermions, so  $n_d = 2$  in the 2HDM. The running of the quartic couplings of  $\lambda_i$ 's is different according to the type. First, we write the  $\beta$  functions in terms of the common part  $c_i$  and the type-dependent part  $h_i$  as

$$16\pi^2\beta_{\lambda_i}^{\text{type}} = c_i + h_i^{\text{type}}, \quad (i = 1, \dots, 5). \quad (\text{A4})$$

The common parts for  $\lambda_i$ 's are

$$c_1 = 12\lambda_1^2 + 4\lambda_3^2 + 4\lambda_3\lambda_4 + 2\lambda_4^2 + 2\lambda_5^2 + \frac{3}{4}(3g^4 + g'^4 + 2g^2g'^2) - 3\lambda_1(3g^2 + g'^2), \quad (\text{A5})$$

$$c_2 = 12\lambda_2^2 + 4\lambda_3^2 + 4\lambda_3\lambda_4 + 2\lambda_4^2 + 2\lambda_5^2 + \frac{3}{4}(3g^4 + g'^4 + 2g^2g'^2) - 3\lambda_2(3g^2 + g'^2) \\ + 12y_t^2\lambda_2 - 12y_t^4,$$

$$c_3 = (\lambda_1 + \lambda_2)(6\lambda_3 + 2\lambda_4) + 4\lambda_3^2 + 2\lambda_4^2 + 2\lambda_5^2 + \frac{3}{4}(3g^4 + g'^4 - 2g^2g'^2) - 3\lambda_3(3g^2 + g'^2) \\ + 2(3y_t^2 + 3y_b^2 + y_\tau^2)\lambda_3,$$

$$c_4 = 2(\lambda_1 + \lambda_2)\lambda_4 + 8\lambda_3\lambda_4 + 4\lambda_4^2 + 8\lambda_5^2 + 3g^2g'^2 - 3(3g^2 + g'^2)\lambda_4 \\ + 2(3y_t^2 + 3y_b^2 + y_\tau^2)\lambda_4,$$

$$c_5 = 2(\lambda_1 + \lambda_2 + 4\lambda_3 + 6\lambda_4)\lambda_5 - 3\lambda_5(3g^2 + g'^2) + 2(3y_t^2 + 3y_b^2 + y_\tau^2)\lambda_5.$$

The  $h_i$ 's in type I are

$$h_1^I = h_3^I = h_4^I = h_5^I = 0, \quad (\text{A6})$$

$$h_2^I = 4(3y_b^2 + y_\tau^2)\lambda_2 - 4(3y_b^4 + y_\tau^4).$$

The Yukawa couplings of the top quark, bottom quark, and tau lepton ( $y_t$ ,  $y_b$ , and  $y_\tau$ ) are running with the  $\beta$  functions of

$$16\pi^2\beta_{y_f}^{\text{type}} = c_{y_f} + h_{y_f}^{\text{type}}, \quad (f = t, b, \tau), \quad (\text{A7})$$

where the common parts are

$$c_{y_t} = \left( -8g_s^2 - \frac{9}{4}g^2 - \frac{17}{12}g'^2 + \frac{9}{2}y_t^2 \right) y_t, \quad (\text{A8})$$

$$c_{y_b} = \left( -8g_s^2 - \frac{9}{4}g^2 - \frac{5}{12}g'^2 + \frac{3}{2}y_t^2 + \frac{9}{2}y_b^2 \right) y_b, \quad (\text{A9})$$

$$c_{y_\tau} = \left( -\frac{9}{4}g^2 - \frac{15}{4}g'^2 + \frac{5}{2}y_\tau^2 \right) y_\tau,$$

and the type-dependent parts are

$$h_{y_t}^I = \left( \frac{3}{2}y_b^2 + y_\tau^2 \right) y_t, \quad h_{y_b}^I = y_\tau^2 y_b, \quad h_{y_\tau}^I = 3(y_t^2 + y_b^2) y_\tau. \quad (\text{A10})$$

The initial conditions of the Yukawa coupling are set at the top quark mass scale  $m_t^{\text{pole}}$  [26] as

$$y_t(m_t^{\text{pole}}) = \frac{\sqrt{2}m_t}{v s_\beta} \left\{ 1 - \frac{4}{3\pi}\alpha_s(m_t) \right\}, \quad (\text{A11})$$

$$y_b(m_t^{\text{pole}}) = \frac{\sqrt{2}m_b}{v s_\beta},$$

$$y_\tau(m_t^{\text{pole}}) = \frac{\sqrt{2}m_\tau}{v s_\beta}.$$

- 
- [1] J. Ellis, *SMEFT Constraints on New Physics beyond the Standard Model*, in *Beyond Standard Model: From Theory to Experiment*, 5, 2021. [2105.14942](#). DOI.
- [2] ATLAS collaboration, G. Aad et al., *Measurements of  $WH$  and  $ZH$  production in the  $H \rightarrow b\bar{b}$  decay channel in  $pp$  collisions at 13 TeV with the ATLAS detector*, *Eur. Phys. J. C* **81** (2021) 178, [[2007.02873](#)].
- [3] ATLAS collaboration, G. Aad et al., *Measurements of Higgs bosons decaying to bottom quarks from vector boson fusion production with the ATLAS experiment at  $\sqrt{s} = 13$  TeV*, *Eur. Phys. J. C* **81** (2021) 537, [[2011.08280](#)].
- [4] CMS collaboration, A. M. Sirunyan et al., *Inclusive search for highly boosted Higgs bosons decaying to bottom quark-antiquark pairs in proton-proton collisions at  $\sqrt{s} = 13$  TeV*, *JHEP* **12** (2020) 085, [[2006.13251](#)].
- [5] ATLAS collaboration, *Study of Higgs-boson production with large transverse momentum using the  $H \rightarrow b\bar{b}$  decay with the ATLAS detector*, [<http://cds.cern.ch/record/2759284>].
- [6] CMS collaboration, A. Tumasyan et al., *Measurement of the inclusive and differential Higgs boson production cross sections in the decay mode to a pair of  $\tau$  leptons in  $pp$  collisions at  $\sqrt{s} = 13$  TeV*, *Phys. Rev. Lett.* **128** (2022) 081805, [[2107.11486](#)].
- [7] ATLAS collaboration, *Measurement of the Higgs boson decaying to  $b$ -quarks produced in association with a top-quark pair in  $pp$  collisions at  $\sqrt{s} = 13$  TeV with the ATLAS detector*, .
- [8] ATLAS collaboration, *Measurements of gluon fusion and vector-boson-fusion production of the Higgs boson in  $H \rightarrow WW^* \rightarrow e\nu\mu\nu$  decays using  $pp$  collisions at  $\sqrt{s} = 13$  TeV with the ATLAS detector*, [<http://cds.cern.ch/record/2743685>].
- [9] ATLAS collaboration, *Measurement of the properties of Higgs boson production at  $\sqrt{s}=13$  TeV in the  $H \rightarrow \gamma\gamma$  channel using 139  $\text{fb}^{-1}$  of  $pp$  collision data with the ATLAS experiment*, [<http://cds.cern.ch/record/2725727>].
- [10] CMS collaboration, A. M. Sirunyan et al., *Measurements of production cross sections of the Higgs boson in the four-lepton final state in proton-proton collisions at  $\sqrt{s} = 13$  TeV*, *Eur. Phys. J. C* **81** (2021) 488, [[2103.04956](#)].
- [11] ATLAS collaboration, G. Aad et al., *Measurements of the Higgs boson inclusive and differential fiducial cross sections in the  $4\ell$  decay channel at  $\sqrt{s} = 13$  TeV*, *Eur. Phys. J. C* **80** (2020) 942, [[2004.03969](#)].
- [12] ATLAS collaboration, G. Aad et al., *Higgs boson production cross-section measurements and their EFT interpretation in the  $4\ell$  decay channel at  $\sqrt{s} = 13$  TeV with the ATLAS detector*, *Eur. Phys. J. C* **80** (2020) 957, [[2004.03447](#)].
- [13] ATLAS collaboration, *A combination of measurements of Higgs boson production and decay using up to 139  $\text{fb}^{-1}$  of proton-proton collision data at  $\sqrt{s} = 13$  TeV collected with the ATLAS experiment*, [<http://cds.cern.ch/record/2725733>].

- [14] ATLAS collaboration, G. Aad et al., *A search for the dimuon decay of the Standard Model Higgs boson with the ATLAS detector*, *Phys. Lett. B* **812** (2021) 135980, [2007.07830].
- [15] CMS collaboration, A. M. Sirunyan et al., *Evidence for Higgs boson decay to a pair of muons*, *JHEP* **01** (2021) 148, [2009.04363].
- [16] ATLAS collaboration, *Direct constraint on the Higgs-charm coupling from a search for Higgs boson decays to charm quarks with the ATLAS detector*, [<http://cds.cern.ch/record/2771724>].
- [17] N. Turok and J. Zadrozny, *Electroweak baryogenesis in the two doublet model*, *Nucl. Phys. B* **358** (1991) 471–493.
- [18] A. G. Cohen, D. B. Kaplan and A. E. Nelson, *Spontaneous baryogenesis at the weak phase transition*, *Phys. Lett. B* **263** (1991) 86–92.
- [19] V. Zarikas, *The Phase transition of the two Higgs extension of the standard model*, *Phys. Lett. B* **384** (1996) 180–184, [[hep-ph/9509338](http://arxiv.org/abs/hep-ph/9509338)].
- [20] J. M. Cline and P.-A. Lemieux, *Electroweak phase transition in two Higgs doublet models*, *Phys. Rev. D* **55** (1997) 3873–3881, [[hep-ph/9609240](http://arxiv.org/abs/hep-ph/9609240)].
- [21] L. Fromme, S. J. Huber and M. Seniuch, *Baryogenesis in the two-Higgs doublet model*, *JHEP* **11** (2006) 038, [[hep-ph/0605242](http://arxiv.org/abs/hep-ph/0605242)].
- [22] M. E. Machacek and M. T. Vaughn, *Two Loop Renormalization Group Equations in a General Quantum Field Theory. 1. Wave Function Renormalization*, *Nucl. Phys. B* **222** (1983) 83–103.
- [23] M. E. Machacek and M. T. Vaughn, *Two Loop Renormalization Group Equations in a General Quantum Field Theory. 2. Yukawa Couplings*, *Nucl. Phys. B* **236** (1984) 221–232.
- [24] M. E. Machacek and M. T. Vaughn, *Two Loop Renormalization Group Equations in a General Quantum Field Theory. 3. Scalar Quartic Couplings*, *Nucl. Phys. B* **249** (1985) 70–92.
- [25] M.-x. Luo, H.-w. Wang and Y. Xiao, *Two loop renormalization group equations in general gauge field theories*, *Phys. Rev. D* **67** (2003) 065019, [[hep-ph/0211440](http://arxiv.org/abs/hep-ph/0211440)].
- [26] D. Das and I. Saha, *Search for a stable alignment limit in two-Higgs-doublet models*, *Phys. Rev. D* **91** (2015) 095024, [[1503.02135](http://arxiv.org/abs/1503.02135)].
- [27] H. E. Haber and R. Hempfling, *The Renormalization group improved Higgs sector of the minimal supersymmetric model*, *Phys. Rev. D* **48** (1993) 4280–4309, [[hep-ph/9307201](http://arxiv.org/abs/hep-ph/9307201)].
- [28] W. Grimus and L. Lavoura, *Renormalization of the neutrino mass operators in the multi-Higgs-doublet standard model*, *Eur. Phys. J. C* **39** (2005) 219–227, [[hep-ph/0409231](http://arxiv.org/abs/hep-ph/0409231)].
- [29] D. Chowdhury and O. Eberhardt, *Global fits of the two-loop renormalized Two-Higgs-Doublet model with soft  $Z_2$  breaking*, *JHEP* **11** (2015) 052, [[1503.08216](http://arxiv.org/abs/1503.08216)].
- [30] P. Basler, P. M. Ferreira, M. Mühlleitner and R. Santos, *High scale impact in alignment and decoupling in two-Higgs doublet models*, *Phys. Rev. D* **97** (2018) 095024, [[1710.10410](http://arxiv.org/abs/1710.10410)].
- [31] M. E. Krauss, T. Opferkuch and F. Staub, *The Ultraviolet Landscape of Two-Higgs Doublet Models*, *Eur. Phys. J. C* **78** (2018) 1020, [[1807.07581](http://arxiv.org/abs/1807.07581)].
- [32] J. Oredsson and J. Rathsmann,  *$Z_2$  breaking effects in 2-loop RG evolution of 2HDM*, *JHEP* **02** (2019) 152, [[1810.02588](http://arxiv.org/abs/1810.02588)].
- [33] M. Aiko and S. Kanemura, *New scenario for aligned Higgs couplings originated from the twisted*

- custodial symmetry at high energies*, *JHEP* **02** (2021) 046, [2009.04330].
- [34] A. Dey, J. Lahiri and B. Mukhopadhyaya, *Muon  $g-2$  and a type- $X$  two-Higgs-doublet scenario: Some studies in high-scale validity*, *Phys. Rev. D* **106** (2022) 055023, [2106.01449].
- [35] S. Lee, K. Cheung, J. Kim, C.-T. Lu and J. Song, *Status of the two-Higgs-doublet model in light of the CDF  $m_W$  measurement*, *Phys. Rev. D* **106** (2022) 075013, [2204.10338].
- [36] J. Kim, S. Lee, P. Sanyal and J. Song, *CDF  $W$ -boson mass and muon  $g-2$  in a type- $X$  two-Higgs-doublet model with a Higgs-phobic light pseudoscalar*, *Phys. Rev. D* **106** (2022) 035002, [2205.01701].
- [37] J. Kim, S. Lee, J. Song and P. Sanyal, *Fermiophobic light Higgs boson in the type- $I$  two-Higgs-doublet model*, *Phys. Lett. B* **834** (2022) 137406, [2207.05104].
- [38] P. M. Ferreira, R. Santos, M. Sher and J. P. Silva, *Could the LHC two-photon signal correspond to the heavier scalar in two-Higgs-doublet models?*, *Phys. Rev. D* **85** (2012) 035020, [1201.0019].
- [39] S. Chang, S. K. Kang, J.-P. Lee and J. Song, *Higgs potential and hidden light Higgs scenario in two Higgs doublet models*, *Phys. Rev. D* **92** (2015) 075023, [1507.03618].
- [40] A. Jueid, J. Kim, S. Lee and J. Song, *Type- $X$  two-Higgs-doublet model in light of the muon  $g-2$ : Confronting Higgs boson and collider data*, *Phys. Rev. D* **104** (2021) 095008, [2104.10175].
- [41] G. C. Branco, P. M. Ferreira, L. Lavoura, M. N. Rebelo, M. Sher and J. P. Silva, *Theory and phenomenology of two-Higgs-doublet models*, *Phys. Rept.* **516** (2012) 1–102, [1106.0034].
- [42] S. L. Glashow and S. Weinberg, *Natural Conservation Laws for Neutral Currents*, *Phys. Rev. D* **15** (1977) 1958.
- [43] E. A. Paschos, *Diagonal Neutral Currents*, *Phys. Rev. D* **15** (1977) 1966.
- [44] H. E. Haber and D. O’Neil, *Basis-independent methods for the two-Higgs-doublet model. II. The Significance of  $\tan\beta$* , *Phys. Rev. D* **74** (2006) 015018, [hep-ph/0602242].
- [45] J. Song and Y. W. Yoon,  *$W\gamma$  decay of the elusive charged Higgs boson in the two-Higgs-doublet model with vectorlike fermions*, *Phys. Rev. D* **100** (2019) 055006, [1904.06521].
- [46] S. Kanemura, Y. Okada, H. Taniguchi and K. Tsumura, *Indirect bounds on heavy scalar masses of the two-Higgs-doublet model in light of recent Higgs boson searches*, *Phys. Lett. B* **704** (2011) 303–307, [1108.3297].
- [47] J. Bernon, J. F. Gunion, H. E. Haber, Y. Jiang and S. Kraml, *Scrutinizing the alignment limit in two-Higgs-doublet models:  $m_h=125$  GeV*, *Phys. Rev. D* **92** (2015) 075004, [1507.00933].
- [48] J. Bernon, J. F. Gunion, H. E. Haber, Y. Jiang and S. Kraml, *Scrutinizing the alignment limit in two-Higgs-doublet models. II.  $m_H=125$  GeV*, *Phys. Rev. D* **93** (2016) 035027, [1511.03682].
- [49] T. Plehn, M. Spira and P. M. Zerwas, *Pair production of neutral Higgs particles in gluon-gluon collisions*, *Nucl. Phys. B* **479** (1996) 46–64, [hep-ph/9603205].
- [50] A. Djouadi, W. Kilian, M. Muhlleitner and P. M. Zerwas, *Production of neutral Higgs boson pairs at LHC*, *Eur. Phys. J. C* **10** (1999) 45–49, [hep-ph/9904287].
- [51] V. Barger, L. L. Everett, C. B. Jackson and G. Shaughnessy, *Higgs-Pair Production and Measurement of the Triscalar Coupling at LHC(8,14)*, *Phys. Lett. B* **728** (2014) 433–436, [1311.2931].
- [52] S. Dawson, A. Ismail and I. Low, *What’s in the loop? The anatomy of double Higgs production*,

- Phys. Rev. D* **91** (2015) 115008, [1504.05596].
- [53] K. Cheung, A. Jueid, C.-T. Lu, J. Song and Y. W. Yoon, *Disentangling new physics effects on nonresonant Higgs boson pair production from gluon fusion*, *Phys. Rev. D* **103** (2021) 015019, [2003.11043].
- [54] A. Jueid, J. Kim, S. Lee and J. Song, *Studies of nonresonant Higgs pair production at electron-proton colliders*, *Phys. Lett. B* **819** (2021) 136417, [2102.12507].
- [55] I. P. Ivanov, *Minkowski space structure of the Higgs potential in 2HDM*, *Phys. Rev. D* **75** (2007) 035001, [hep-ph/0609018].
- [56] I. F. Ginzburg and I. P. Ivanov, *Tree-level unitarity constraints in the most general 2HDM*, *Phys. Rev. D* **72** (2005) 115010, [hep-ph/0508020].
- [57] S. Kanemura and K. Yagyu, *Unitarity bound in the most general two Higgs doublet model*, *Phys. Lett. B* **751** (2015) 289–296, [1509.06060].
- [58] A. Arhrib, *Unitarity constraints on scalar parameters of the standard and two Higgs doublets model*, in *Workshop on Noncommutative Geometry, Superstrings and Particle Physics*, 12, 2000. hep-ph/0012353.
- [59] I. P. Ivanov, *General two-order-parameter Ginzburg-Landau model with quadratic and quartic interactions*, *Phys. Rev. E* **79** (2009) 021116, [0802.2107].
- [60] A. Barroso, P. M. Ferreira, I. P. Ivanov, R. Santos and J. P. Silva, *Evading death by vacuum*, *Eur. Phys. J. C* **73** (2013) 2537, [1211.6119].
- [61] A. Barroso, P. M. Ferreira, I. P. Ivanov and R. Santos, *Metastability bounds on the two Higgs doublet model*, *JHEP* **06** (2013) 045, [1303.5098].
- [62] D. Eriksson, J. Rathsmann and O. Stal, *2HDMC: Two-Higgs-Doublet Model Calculator Physics and Manual*, *Comput. Phys. Commun.* **181** (2010) 189–205, [0902.0851].
- [63] V. Branchina, F. Contino and P. M. Ferreira, *Electroweak vacuum lifetime in two Higgs doublet models*, *JHEP* **11** (2018) 107, [1807.10802].
- [64] M. E. Peskin and T. Takeuchi, *Estimation of oblique electroweak corrections*, *Phys. Rev. D* **46** (1992) 381–409.
- [65] H.-J. He, N. Polonsky and S.-f. Su, *Extra families, Higgs spectrum and oblique corrections*, *Phys. Rev. D* **64** (2001) 053004, [hep-ph/0102144].
- [66] W. Grimus, L. Lavoura, O. M. Ogreid and P. Osland, *The Oblique parameters in multi-Higgs-doublet models*, *Nucl. Phys. B* **801** (2008) 81–96, [0802.4353].
- [67] PARTICLE DATA GROUP collaboration, P. A. Zyla et al., *Review of Particle Physics*, *PTEP* **2020** (2020) 083C01.
- [68] PARTICLE DATA GROUP collaboration, R. L. Workman et al., *Review of Particle Physics*, *PTEP* **2022** (2022) 083C01.
- [69] A. Arbey, F. Mahmoudi, O. Stal and T. Stefaniak, *Status of the Charged Higgs Boson in Two Higgs Doublet Models*, *Eur. Phys. J. C* **78** (2018) 182, [1706.07414].
- [70] P. Sanyal, *Limits on the Charged Higgs Parameters in the Two Higgs Doublet Model using CMS  $\sqrt{s} = 13$  TeV Results*, *Eur. Phys. J. C* **79** (2019) 913, [1906.02520].



- [71] M. Misiak and M. Steinhauser, *Weak radiative decays of the B meson and bounds on  $M_{H^\pm}$  in the Two-Higgs-Doublet Model*, *Eur. Phys. J. C* **77** (2017) 201, [1702.04571].
- [72] P. Bechtle, S. Heinemeyer, T. Klingl, T. Stefaniak, G. Weiglein and J. Wittbrodt, *HiggsSignals-2: Probing new physics with precision Higgs measurements in the LHC 13 TeV era*, *Eur. Phys. J. C* **81** (2021) 145, [2012.09197].
- [73] ATLAS collaboration, M. Aaboud et al., *Search for Higgs bosons produced via vector-boson fusion and decaying into bottom quark pairs in  $\sqrt{s} = 13$  TeV pp collisions with the ATLAS detector*, *Phys. Rev. D* **98** (2018) 052003, [1807.08639].
- [74] ATLAS collaboration, M. Aaboud et al., *Measurements of gluon-gluon fusion and vector-boson fusion Higgs boson production cross-sections in the  $H \rightarrow WW^* \rightarrow e\nu\mu\nu$  decay channel in pp collisions at  $\sqrt{s} = 13$  TeV with the ATLAS detector*, *Phys. Lett. B* **789** (2019) 508–529, [1808.09054].
- [75] ATLAS collaboration, M. Aaboud et al., *Cross-section measurements of the Higgs boson decaying into a pair of  $\tau$ -leptons in proton-proton collisions at  $\sqrt{s} = 13$  TeV with the ATLAS detector*, *Phys. Rev. D* **99** (2019) 072001, [1811.08856].
- [76] ATLAS collaboration, G. Aad et al., *Higgs boson production cross-section measurements and their EFT interpretation in the  $4\ell$  decay channel at  $\sqrt{s} = 13$  TeV with the ATLAS detector*, *Eur. Phys. J. C* **80** (2020) 957, [2004.03447].
- [77] CMS collaboration, A. M. Sirunyan et al., *Search for  $t\bar{t}H$  production in the  $H \rightarrow b\bar{b}$  decay channel with leptonic  $t\bar{t}$  decays in proton-proton collisions at  $\sqrt{s} = 13$  TeV*, *JHEP* **03** (2019) 026, [1804.03682].
- [78] CMS collaboration, A. M. Sirunyan et al., *Search for the Higgs boson decaying to two muons in proton-proton collisions at  $\sqrt{s} = 13$  TeV*, *Phys. Rev. Lett.* **122** (2019) 021801, [1807.06325].
- [79] CMS collaboration, *Measurements of properties of the Higgs boson in the four-lepton final state in proton-proton collisions at  $\sqrt{s} = 13$  TeV*, [<http://cds.cern.ch/record/2668684>].
- [80] CMS collaboration, *Measurements of differential Higgs boson production cross sections in the leptonic  $WW$  decay mode at  $\sqrt{s} = 13$  TeV*, [<http://cds.cern.ch/record/2691268>].
- [81] P. Bechtle, D. Dercks, S. Heinemeyer, T. Klingl, T. Stefaniak, G. Weiglein et al., *HiggsBounds-5: Testing Higgs Sectors in the LHC 13 TeV Era*, *Eur. Phys. J. C* **80** (2020) 1211, [2006.06007].
- [82] CDF collaboration, T. Aaltonen et al., *High-precision measurement of the W boson mass with the CDF II detector*, *Science* **376** (2022) 170–176.
- [83] C.-T. Lu, L. Wu, Y. Wu and B. Zhu, *Electroweak precision fit and new physics in light of the W boson mass*, *Phys. Rev. D* **106** (2022) 035034, [2204.03796].
- [84] Y.-Z. Fan, T.-P. Tang, Y.-L. S. Tsai and L. Wu, *Inert Higgs Dark Matter for CDF II W-Boson Mass and Detection Prospects*, *Phys. Rev. Lett.* **129** (2022) 091802, [2204.03693].
- [85] C.-R. Zhu, M.-Y. Cui, Z.-Q. Xia, Z.-H. Yu, X. Huang, Q. Yuan et al., *Explaining the GeV antiproton/ $\gamma$ -ray excesses and W-boson mass anomaly in an inert two Higgs doublet model*, [2204.03767].
- [86] B.-Y. Zhu, S. Li, J.-G. Cheng, R.-L. Li and Y.-F. Liang, *Using gamma-ray observation of dwarf*

- spheroidal galaxy to test a dark matter model that can interpret the  $W$ -boson mass anomaly, [2204.04688](#).
- [87] H. Song, W. Su and M. Zhang, *Electroweak phase transition in 2HDM under Higgs,  $Z$ -pole, and  $W$  precision measurements*, *JHEP* **10** (2022) 048, [[2204.05085](#)].
- [88] H. Bahl, J. Braathen and G. Weiglein, *New physics effects on the  $W$ -boson mass from a doublet extension of the SM Higgs sector*, *Phys. Lett. B* **833** (2022) 137295, [[2204.05269](#)].
- [89] Y. Heo, D.-W. Jung and J. S. Lee, *Impact of the CDF  $W$ -mass anomaly on two Higgs doublet model*, *Phys. Lett. B* **833** (2022) 137274, [[2204.05728](#)].
- [90] K. S. Babu, S. Jana and V. P. K., *Correlating  $W$ -Boson Mass Shift with Muon  $g-2$  in the Two Higgs Doublet Model*, *Phys. Rev. Lett.* **129** (2022) 121803, [[2204.05303](#)].
- [91] T. Biekötter, S. Heinemeyer and G. Weiglein, *Excesses in the low-mass Higgs-boson search and the  $W$ -boson mass measurement*, [2204.05975](#).
- [92] Y. H. Ahn, S. K. Kang and R. Ramos, *Implications of New CDF-II  $W$  Boson Mass on Two Higgs Doublet Model*, *Phys. Rev. D* **106** (2022) 055038, [[2204.06485](#)].
- [93] X.-F. Han, F. Wang, L. Wang, J. M. Yang and Y. Zhang, *Joint explanation of  $W$ -mass and muon  $g-2$  in the 2HDM\**, *Chin. Phys. C* **46** (2022) 103105, [[2204.06505](#)].
- [94] G. Arcadi and A. Djouadi, *2HD plus light pseudoscalar model for a combined explanation of the possible excesses in the CDF  $MW$  measurement and  $(g-2)\mu$  with dark matter*, *Phys. Rev. D* **106** (2022) 095008, [[2204.08406](#)].
- [95] K. Ghorbani and P. Ghorbani,  *$W$ -boson mass anomaly from scale invariant 2HDM*, *Nucl. Phys. B* **984** (2022) 115980, [[2204.09001](#)].
- [96] A. Broggio, E. J. Chun, M. Passera, K. M. Patel and S. K. Vempati, *Limiting two-Higgs-doublet models*, *JHEP* **11** (2014) 058, [[1409.3199](#)].
- [97] J. Oredsson, *2HDME : Two-Higgs-Doublet Model Evolver*, *Comput. Phys. Commun.* **244** (2019) 409–426, [[1811.08215](#)].
- [98] I. P. Ivanov, *Minkowski space structure of the Higgs potential in 2HDM. II. Minima, symmetries, and topology*, *Phys. Rev. D* **77** (2008) 015017, [[0710.3490](#)].
- [99] A. G. Akeroyd, *Fermiophobic Higgs bosons at the Tevatron*, *Phys. Lett. B* **368** (1996) 89–95, [[hep-ph/9511347](#)].
- [100] A. G. Akeroyd, *Fermiophobic and other nonminimal neutral Higgs bosons at the LHC*, *J. Phys. G* **24** (1998) 1983–1994, [[hep-ph/9803324](#)].
- [101] A. Barroso, L. Brucher and R. Santos, *Is there a light fermiophobic Higgs?*, *Phys. Rev. D* **60** (1999) 035005, [[hep-ph/9901293](#)].
- [102] L. Brucher and R. Santos, *Experimental signatures of fermiophobic Higgs bosons*, *Eur. Phys. J. C* **12** (2000) 87–98, [[hep-ph/9907434](#)].
- [103] A. G. Akeroyd, M. A. Diaz and F. J. Pacheco, *Double fermiophobic Higgs boson production at the CERN LHC and LC*, *Phys. Rev. D* **70** (2004) 075002, [[hep-ph/0312231](#)].
- [104] A. Arhrib, R. Benbrik, R. B. Guedes and R. Santos, *Search for a light fermiophobic Higgs boson produced via gluon fusion at Hadron Colliders*, *Phys. Rev. D* **78** (2008) 075002, [[0805.1603](#)].

- [105] E. L. Berger, Z. Sullivan and H. Zhang, *Associated Higgs plus vector boson test of a fermiophobic Higgs boson*, *Phys. Rev. D* **86** (2012) 015011, [[1203.6645](#)].
- [106] V. Ilisie and A. Pich, *Low-mass fermiophobic charged Higgs phenomenology in two-Higgs-doublet models*, *JHEP* **09** (2014) 089, [[1405.6639](#)].
- [107] A. Delgado, M. Garcia-Pepin, M. Quiros, J. Santiago and R. Vega-Morales, *Diphoton and Di-boson Probes of Fermiophobic Higgs Bosons at the LHC*, *JHEP* **06** (2016) 042, [[1603.00962](#)].
- [108] T. Mondal and P. Sanyal, *Same sign trilepton as signature of charged Higgs in two Higgs doublet model*, *JHEP* **05** (2022) 040, [[2109.05682](#)].
- [109] K. Cheung, A. Jueid, J. Kim, S. Lee, C.-T. Lu and J. Song, *Comprehensive study of the light charged Higgs boson in the type-I two-Higgs-doublet model*, *Phys. Rev. D* **105** (2022) 095044, [[2201.06890](#)].
- [110] M. Forsslund and P. Meade, *High precision higgs from high energy muon colliders*, *JHEP* **08** (2022) 185, [[2203.09425](#)].
- [111] M. Misiak, A. Rehman and M. Steinhauser, *Towards  $\bar{B} \rightarrow X_s \gamma$  at the NNLO in QCD without interpolation in  $m_c$* , *JHEP* **06** (2020) 175, [[2203.09425](#)].
- [112] A. Djouadi, *The Anatomy of electro-weak symmetry breaking. II. The Higgs bosons in the minimal supersymmetric model*, *Phys. Rept.* **459** (2008) 1–241, [[hep-ph/0503173](#)].
- [113] C. Degrande, C. Duhr, B. Fuks, D. Grellscheid, O. Mattelaer and T. Reiter, *UFO - The Universal FeynRules Output*, *Comput. Phys. Commun.* **183** (2012) 1201–1214, [[1108.2040](#)].
- [114] A. Alloul, N. D. Christensen, C. Degrande, C. Duhr and B. Fuks, *FeynRules 2.0 - A complete toolbox for tree-level phenomenology*, *Comput. Phys. Commun.* **185** (2014) 2250–2300, [[1310.1921](#)].
- [115] J. Alwall, M. Herquet, F. Maltoni, O. Mattelaer and T. Stelzer, *MadGraph 5 : Going Beyond*, *JHEP* **06** (2011) 128, [[1106.0522](#)].
- [116] NNPDF collaboration, R. D. Ball et al., *Parton distributions from high-precision collider data*, *Eur. Phys. J. C* **77** (2017) 663, [[1706.00428](#)].
- [117] J. Baglio, A. Djouadi, R. Gröber, M. M. Mühlleitner, J. Quevillon and M. Spira, *The measurement of the Higgs self-coupling at the LHC: theoretical status*, *JHEP* **04** (2013) 151, [[1212.5581](#)].
- [118] ATLAS collaboration, *Measurement prospects of the pair production and self-coupling of the Higgs boson with the ATLAS experiment at the HL-LHC*, [<http://cds.cern.ch/record/2652727>].
- [119] A. Ballestrero, G. Bevilacqua and E. Maina, *A Complete parton level analysis of boson-boson scattering and ElectroWeak Symmetry Breaking in  $lv + \text{four jets}$  production at the LHC*, *JHEP* **05** (2009) 015, [[0812.5084](#)].
- [120] S. Jung, Z. Liu, L.-T. Wang and K.-P. Xie, *Probing Higgs boson exotic decays at the LHC with machine learning*, *Phys. Rev. D* **105** (2022) 035008, [[2109.03294](#)].
- [121] TLEP DESIGN STUDY WORKING GROUP collaboration, M. Bicer et al., *First Look at the Physics Case of TLEP*, *JHEP* **01** (2014) 164, [[1308.6176](#)].
- [122] J. Gao, *CEPC and SppC Status — From the completion of CDR towards TDR*, *Int. J. Mod.*

- Phys. A* **36** (2021) 2142005.
- [123] CEPC STUDY GROUP collaboration, M. Dong et al., *CEPC Conceptual Design Report: Volume 2 - Physics & Detector*, [1811.10545](#).
- [124] R. B. Palmer, J. S. Berg, R. C. Fernow, J. C. Gallardo, H. G. Kirk, Y. Alexahin et al., *A Complete Scheme of Ionization Cooling for a Muon Collider*, *Conf. Proc. C* **070625** (2007) 3193, [[0711.4275](#)].
- [125] J. P. Delahaye, M. Diemoz, K. Long, B. Mansoulié, N. Pastrone, L. Rivkin et al., *Muon Colliders*, [1901.06150](#).
- [126] K. M. Black et al., *Muon Collider Forum Report*, [2209.01318](#).
- [127] T. P. Cheng, E. Eichten and L.-F. Li, *Higgs Phenomena in Asymptotically Free Gauge Theories*, *Phys. Rev. D* **9** (1974) 2259.
- [128] H. Komatsu, *Behavior of the Yukawa and the Quartic Scalar Couplings in Grand Unified Theories*, *Prog. Theor. Phys.* **67** (1982) 1177.